National Technical University of Athens

School of Naval Architecture and Marine Engineering

Laboratory of Marine Engineering

MODELING AND SIMULATION OF THE STARTING PROCEDURE OF A LARGE TWO-STROKE MARINE DIESEL ENGINE

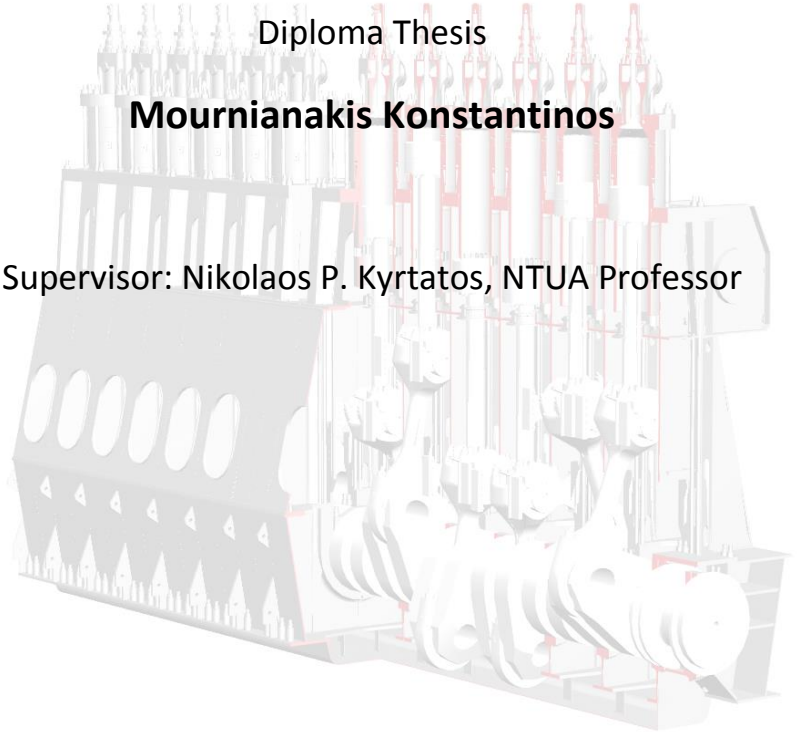

Diploma Thesis

Mournianakis Konstantinos

Supervisor: Nikolaos P. Kyrtatos, NTUA Professor

Athens

November 2015

Abstract

The present thesis focuses on the modeling and the simulation of the starting procedure of a large marine two-stroke diesel engine with direct admission of compressed air into the cylinders, through separate valves fitted on each cylinder. Simulations for a representative propulsion engine are performed to investigate the engine – propeller - ship interaction during the starting phase of the engine. The compressor performance during this phase is also examined.

The main components of the pneumatic starting system and their operation are described in Chapter 2. The models of the main thermodynamic and mechanical elements, that are used to configure the engine structure, are described in Chapter 3. The main components of the starting system are modeled using the thermodynamic elements of the engine simulation code. Furthermore, a simplified model to predict the static friction of the shafting system and the friction torque, as a function of the engine speed, is also introduced in Chapter 4.

During the starting phase of a turbocharged engine, the turbocharging system is operating in off – design points. Thus, it is necessary to adequately model its transient behavior during this phase. The performance prediction of the turbocharger for low load operation is based on the extension of compressor and turbine maps, as it is described in Chapter 5.

A model capable of predicting the transient behavior of a propulsion engine, requires the calculation of the propeller torque demand. Hence, a propeller model capable of estimating the thrust and torque characteristics, in four quadrants of propeller operation, is introduced in Chapter 6. Such a model enables the performance prediction of the propulsion system under any transient operating condition. The performance characteristics of the propeller depend on the ship's axial speed, so a ship surge model is included.

The derived models are integrated into the MOtor THERmodynamics (MOTHER) engine simulation and performance prediction code and are used to simulate the transient behavior of a representative large marine two-stroke diesel engine. Various simulations are performed to investigate the engine – propeller – ship interaction during the starting phase of the engine. The limited engine performance during this phase, due to poor turbocharger performance, is also investigated. Lastly, a crash-stop manoeuvre simulation is performed.

Acknowledgements

First of all, I would like to thank my supervisor, Professor N. P. Kyrtatos, for his guidance, constructive comments and advices throughout the course of his thesis.

Secondly, many thanks are in order to senior Research Engineer of the Laboratory of Marine Engineering, Mr. Tzanos, for his guidance, advice and sharing of experience concerning the MOtor THErmodynamics (MOTHER) engine simulation code.

Last but not least, I would like to thank my colleagues, friends and family for all their support and encouragement throughout the course of his thesis.

Table of Contents

Abstract i

Acknowledgements ii

Table of Contents iii

List of Figures v

List of Tables vii

Nomenclature viii

1 Introduction 1

1.1 Starting Systems Overview 1

1.2 Marine Pneumatic Starting Systems 1

1.3 Motivation and Objectives 3

1.4 Thesis Outline 3

2 Staring System Description 5

2.1 System Overview 5

2.2 Starting Air System 8

2.2.1 Main Starting valve 9

2.2.2 Starting Air Distributor 9

2.2.3 Starting Valve 11

2.3 Starting and Reversing the Engine 12

2.4 Scavenge Air System - Auxiliary Blowers 15

2.5 Regulatory Framework 16

3 Engine Model 19

3.1 Introduction 19

3.2 Marine Diesel Engine Model 19

3.2.1 Flow Receivers 20

3.2.2 Flow Controllers 23

3.2.3 Mechanical Elements 24

4 Starting System Model 25

4.1 Starting Air Receivers 25

4.2 Starting Valve 26

4.3 Friction Model 27
5 Turbocharger Modeling 30
5.1 Compressor Modeling 30
5.1.1 Auxiliary Blower Model 32
5.2 Compressor Map Extension 33
5.3 Turbine Modeling 37
5.4 Turbine Map Extension 39
6 Engine – Propeller - Ship Interaction 41
6.1 Four-Quadrant Propeller Modeling 41
6.2 Propeller Shaft Dynamics 44
6.2.1 Dry propeller inertia 45
6.2.2 Added propeller inertia 46
6.3 Ship Surge Model 47
7 Simulation Setup and Results 50
7.1 Engine Characteristics 50
7.2 Propeller Characteristics 52
7.3 Simulation Setup 55
7.4 Simulation Results 59
8 Conclusions 67
8.1 Discussion 67
8.2 Recommendations for Future Research 68
References 69

List of Figures

Figure 2.1: *Starting and Control Air Systems [2]* 6
Figure 2.2: *Manoeuvring System Diagram [1]* 7
Figure 2.3: *Starting Air System [1]* 8
Figure 2.4: *Diagram of Axial Starting Air Distributor* 10
Figure 2.5: *Operation of Radial Starting Air Distributor for Ahead Starting* 10
Figure 2.6: *Operation of Radial Starting Air Distributor for Astern Starting* 11
Figure 2.7: *Starting Valve Timing for Engine Operation in the Ahead Direction* 12
Figure 2.8: *Fuel Pump Reversing Mechanism [1]* 13
Figure 2.9: *Starting Valve Timing for Engine Operation in the Astern Direction* 13
Figure 2.10: *Sequence Diagram of Reversible Engines [1]* 14
Figure 2.11: *Diagram of the Scavenge Air System [1]* 15
Figure 2.12: *Operation of the Auxiliary Blowers [1]* 16
Figure 4.1: *Friction as a function of Velocity for Low Velocities [6]* 28
Figure 5.1: *Compressor enthalpy versus entropy thermodynamic diagram [5]* 31
Figure 5.2: *Compressor Map Example* 33
Figure 5.3: *Non –Dimensional Compressor Head Coefficient Interpolated Surface using the four lowest Original Constant Speed Lines* 35
Figure 5.4: *Compressor Isentropic Efficiency Surface Interpolation using the four lowest Original Constant Speed Lines* 35
Figure 5.5: *Extrapolated Compressor Constant Speed Lines* 36
Figure 5.6: *Extrapolated Compressor Isentropic Efficiency for Constant Speed* 37
Figure 5.7: *Turbine enthalpy versus entropy thermodynamic diagram [5]* 38
Figure 5.8: *Turbine's Swallowing Capacity Map* 40
Figure 6.1: *Propeller four quadrants of operation [13]* 42
Figure 6.2: *Open Water Test Results for Wageningen B4-70 Screw Series over a range of* P/D *values in four quadrants [13]* 43
Figure 7.1: *MAN B&W S70MC-C7 Engine Cross Section [1]* 51
Figure 7.2: *Turbocharger Unit Casing Diagram [ABB Brochure]* 52
Figure 7.3: *Wageningen B4-70, P/D=1.0 open water characteristics in four quadrants of operation* 53
Figure 7.4: *MAN B&W 6S70MC – Engine Configuration* 55
Figure 7.5: *Engine Configuration for the Simulation of its transient behavior during the Starting Phase* 56
Figure 7.6: *Starting Valve Effective Area as a function of the Crank Angle* 57
Figure 7.7: *Shafting System Frictional Torque Load* 58
Figure 7.8: *Engine Starting Simulation Tests over a range of values for the initial Pressure of the Starting Air Receiver* 59
Figure 7.9: *Engine Starting and Acceleration Simulation* 60

Figure 7.10: *Compressor Poor Performance during Engine Starting and Acceleration Simulation due to low Exhaust Receiver Pressure* 61
Figure 7.11: *Engine – Propeller – Ship Interaction during Starting and Acceleration Simulation* 62
Figure 7.12: *Compressor Performance during Engine Starting and Acceleration Simulation* 63
Figure 7.13: *Robinson Diagram for a Crash-Stop Manoeuvre* 64
Figure 7.14: *Per Cycle Average Compressor Operating Points during Engine Crash-Stop Manoeuvre*.....65
Figure 7.15: *Per Cycle Average Temperature and Pressure Drop, in Exhaust and Scavenge Receiver, respectively*.....66

List of Tables

Table 2.1: *Required Number of Starts for Propulsion Engine(s) [3]* 17
Table 6.1: *Propeller four quadrants of operation* 42
Table 6.2: *Propeller Blade Moment of Inertia Calculation Method [13]* 45
Table 7.1: *MAN B&W 6S70MC-C parameters* 50
Table 7.2: *Phase Angle of each Cylinder* 51
Table 7.3: *Turbocharger Unit Casing Geometry and Weight [ABB Brochure]* 52
Table 7.4: *Propeller Characteristics used in the Simulation Setup* 53
Table 7.5: *Harmonic Coefficients for B4-70, P/D=0.8 four-quadrant open water propeller characteristics [15]* 54
Table 7.6: *Thermodynamic and Mechanical elements of the initial Engine Configuration* 55
Table 7.7: *Thermodynamic and Mechanical Elements added to the initial Engine Configuration* 57
Table 7.8: *Turning Gear Technical Data* 58

Nomenclature

A	area	[m^2]
B	cylinder bore	[m^2]
C_Q^*	propeller torque coefficient	[-]
C_T^*	propeller thrust coefficient	[-]
C_T	ship total resistance coefficient	[-]
c_p	specific heat at constant pressure	[J/(kg·K)]
c_v	specific heat at constant volume	[J/(kg·K)]
D	diameter	[m]
f_s	stoichiometric fuel/air ratio	[-]
J	advance coefficient	[-]
H	total enthalpy	[J]
h	specific enthalpy	[J/kg]
I	polar moment of inertia	[kg· m^2]
M	mach number	[-]
M_s	ship mass	[kg]
M_{added}	ship added mass	[kg]
m	mass	[kg]
$\dot{m}$	mass flow rate	[kg/sec]
N	rotational speed	[rpm]
n	rotational speed	[rps]
p	pressure	[Pa]
Q	heat transfer	[J]
$\dot{Q}$	heat transfer rate	[J]
Q_{fr}	friction torque	[N·m]
Q_p	propeller torque	[N·m]
Q_{st}	static friction torque	[N·m]
R	gas constant	[J/(kg·K)]
R_T	ship total resistance	[N]
r	radius	[m]
S	ship wetted surface	[m^2]
T	temperature	[K]
T_p	propeller thrust	[N]
t	time	[sec]
U	internal energy	[J]
u	specific internal energy	[J/kg]
u_{dif}	gas velocity exiting turbine diffuser	[m/sec]
u_{tip}	compressor impeller tip linear velocity	[m/sec]
V	volume	[m^3]

$\dot{V}$	volumetric flow rate	[m^3/sec]
V_a	advance velocity	[m/sec]
V_r	relative advance velocity	[m/sec]
V_s	ship velocity	[m/sec]
W	work transfer	[J]
$\dot{W}$	work transfer rate	[W]

Greek symbols

β	advance angle	[rad]
γ	ratio of specific heats	[-]
θ	crank angle	[rad]
η	isentropic efficiency	[-]
π	compressor working pressure ratio	[-]
ρ	density	[kg/m^3]
τ	torque	[N·m]
Φ	compressor flow coefficient	[-]
φ	equivalence ratio	[-]
Ψ	compressor head coefficient	[-]
ω	angular speed	[rad/sec]

Subscripts

o	total conditions
0	propeller disk
1	compressor inlet
2	compressor outlet
3	turbine inlet
4	turbine outlet
100%	engine steady state condition load percentage
C	compressor
cr	critical
cor	corrected
d	downstream
dif	turbine diffuser
e	effective
eng	engine
eq	equivalent
f	fuel
fb	burnt fuel
h	propeller hub
imp	compressor impeller
MCR	Maximum Continuous Rating

p	propeller
ref	reference conditions
s	isentropic
sf	surface
st	standard conditions
sw	sea water
T	turbine
tip	compressor impeller tip
tot	total
$t-t$	total – to – total conditions
$t-s$	total – to – static conditions
u	upstream

1 Introduction

1.1 Starting Systems Overview

All internal combustion engines, regardless of their output power, rely on some sort of external power system to start. The main task of the starting system, irrespective of its power source, is to accelerate the engine and produce sufficient cylinder pressure and temperature for ignition of the fuel. Then, the engine should be able to fire and run up to self-sustaining speed and the starting system can be disconnected.

The first internal combustion engines relied on various external power sources and starting techniques including wind-up springs, gunpowder cylinders and human-powered techniques, such as a removable hand crank, pulling on an airplane propeller or pulling a cord wound around a pulley. Some of these techniques are still being used today to start engines with low power output, such as outboard boat engines, motorcycle engines and chainsaw engines. Though, the electric starter motor is the most common type of starting system used on gasoline engines and small diesel engines.

While the output power of internal combustion engines is getting larger and larger, the aforementioned starting techniques become insufficient and impractical. Consequently, other systems, attaining much bigger power to size and power to weight ratios, are preferred. Large two-stroke or four-stroke diesel engines use pneumatic starting systems. For large engines, like the ones used as the propulsion engines of ships, the power demand is so vast that any other system powerful enough to accelerate the engine would be practically inapplicable.

The present thesis focuses on the modeling of the starting system of a representative large marine two-stroke diesel engine used as the main engine of a merchant ship. This type of engines use a pneumatic starting system with direct admission of compressed air into the cylinders through separate valves.

1.2 Marine Pneumatic Starting Systems

All starting systems work on the same principle, power has to be stored and then released in order to accelerate the engine. The exact type of starting system that will be used is a unique decision for each specific installation, based on many

factors and requirements, such as operating conditions, safety, regulations, cost, power to size and power to weight ratios.

The most common starting system for large propulsion engines is powered by compressed air. The high power to size and power to weight ratios can easily explain the dominance of pneumatic systems. If a conventional electric starter motor, with sufficient power to start a large marine engine was used, it would be too large and too heavy. Moreover, compressed air systems find more applications onboard ships, such as control air systems, pneumatic valves and tools, etc. Lastly, the use of a pneumatic starting system offers an increased level of safety for the ship's engine room.

Pneumatic starting systems currently used to start medium and large diesel engines can be divided into two main categories:

- Pneumatic motors geared to the engine flywheel
- Systems with direct admission of compressed air into the cylinders through separate valves

The system of the first type is usually used to start medium four-stroke diesel engines. Pneumatic starting motors are normally powered by compressed air at pressure of 10 - 30 bar and they convert the energy of the compressed air to mechanical work through either linear or rotary motion.

The pneumatic starting system of the second type is used to start large propulsion engines. This type of system is not ideal for smaller diesel engines because it results in too much cooling of the cylinder cover during starting. Also, the cylinder head needs to be large enough to support the installation of the extra valve needed for the starting air system. This type of system can be used on either two-stroke or four-stroke engines without regard to the type of the engine, reversible or non-reversible.

The direct admission of compressed air into the cylinders results in a rapid engine acceleration. The increased rate of compression, during the compression stroke of the cylinder, reduces the leakage of air past the piston rings and the thermal losses to the cylinder cover. Therefore, the temperature at the end of the compression stroke will be raised above the self-ignition temperature of the fuel employed.

1.3 Motivation and Objectives

The configuration of the starting air system of a large propulsion engine is quite complicated because of the many pneumatic controls involved, especially when the engine is of the reversible type. Hence, the main components of the starting configuration should be identified and their operation should be understood. Moreover, a model capable of predicting the transient behavior of the engine during its starting phase should be developed.

In addition, during the starting phase of a turbocharged engine, the turbocharger(s) are operating far from their normal operating points. So, the turbocharger performance for low load operation should be modeled. The impact of the poor compressor performance on the transient behavior of the engine, during its starting phase, should also be examined.

A model capable of predicting the performance of a propulsion engine during transient loading requires the calculation of the propeller torque demand at any instant. Thus, a propeller model has to be introduced, along with a ship surge model. This way, the engine – ship – propeller interaction can also be investigated.

The main objective of the present thesis is to adequately model the starting air system of the engine and predict the engine transient behavior during its starting phase. The derived models are to be integrated into a very detailed engine performance simulation software that has been under development for a number of years in the Laboratory of Marine Engineering, called MOtor THERmodynamics (MOTHER).

1.4 Thesis Outline

In this section, an overview of the forthcoming Chapters is presented. First of all, a detailed description of the engine starting configuration and the operation of its most important components, are presented in the following Chapter 2. The relevant regulatory framework is also mentioned.

The models of the basic thermodynamic and mechanical elements configuring the engine structure in the MOTHER engine simulation code, are presented in Chapter 3.

Chapter 4 presents the modeling of the main components of the starting air system. The friction model that is used to calculate the friction torque, along with the assumptions and simplifications made, are presented as well.

Chapter 5 describes the model of the turbocharger. The performance prediction of both the turbine and the compressor for low load operation is based on the extrapolation of their performance maps, which is also presented.

In Chapter 6, the model used to predict the propeller performance is described. A simple ship surge model is also introduced to account for the ship - propeller interaction.

In Chapter 7, the main characteristics of the propulsion plant that is used to simulate the engine performance during its initial startup, are presented. Then, the main simulation results concerning engine performance prediction, as well as the impact of the compressor performance, are presented. The engine – propeller – ship interaction is also examined during a crash – stop manoeuvre.

Finally, in Chapter 8, the findings and conclusions of this thesis are summarized. Some suggestions for future work are also proposed.

2 Staring System Description

All current large propulsion engines use a pneumatic starting system. The advantages of such a system were stated in the introductory chapter. Briefly, large marine two-stroke engines start with the direct admission of compressed air into the cylinders through a separate starting valve fitted on each cylinder cap.

2.1 System Overview

For camshaft controlled two-stroke engines of the reversible type, the starting system configuration is quite complicated. Apart from the starting air system, there is also a complicated control air system because most engine operations are controlled pneumatically. Control air is used to start or stop the engine, to alternate the engine's starting direction between ahead and astern, to control the timing of the starting valves and operate the exhaust valve air springs. In electronically controlled two-stroke engines, instead, some of the aforementioned pneumatic control systems have been replaced by solenoid valves controlled by the Engine Control Unit.

A diagram of a starting and control air system, corresponding to a representative marine installation, is presented in Figure 2.1. Starting air receivers are charged with compressed air to the maximum operation pressure of 30 bar by the air compressors. Through inlet "A", compressed air is supplied to the main engine for starting purposes. Another line fitted with a reduction station supplies the engine with filtered compressed air at 7 bar. Through inlet "B", the engine is supplied with control air for the manoeuvring system and the exhaust valve air springs, while through inlet "C" safety air is supplied for emergency stop [1]. Through a reduction valve, compressed air at 10 bar is supplied to the engine, through inlet "AP", for turbocharger cleaning (soft blast), while a minor volume is used for fuel valve testing [1]. Lastly, the auxiliary engines are supplied with starting and control air from the starting air receivers. An emergency air compressor and air receiver are installed for emergency start of the auxiliary engines.

The air compressors are fitted with an oil and water separator, in case of high-humidity atmospheric air being sucked in by the compressors. The capacity of the air compressors and the volume of the starting air receivers are suggested by the engine manufacturer so as to fulfill the corresponding requirements.

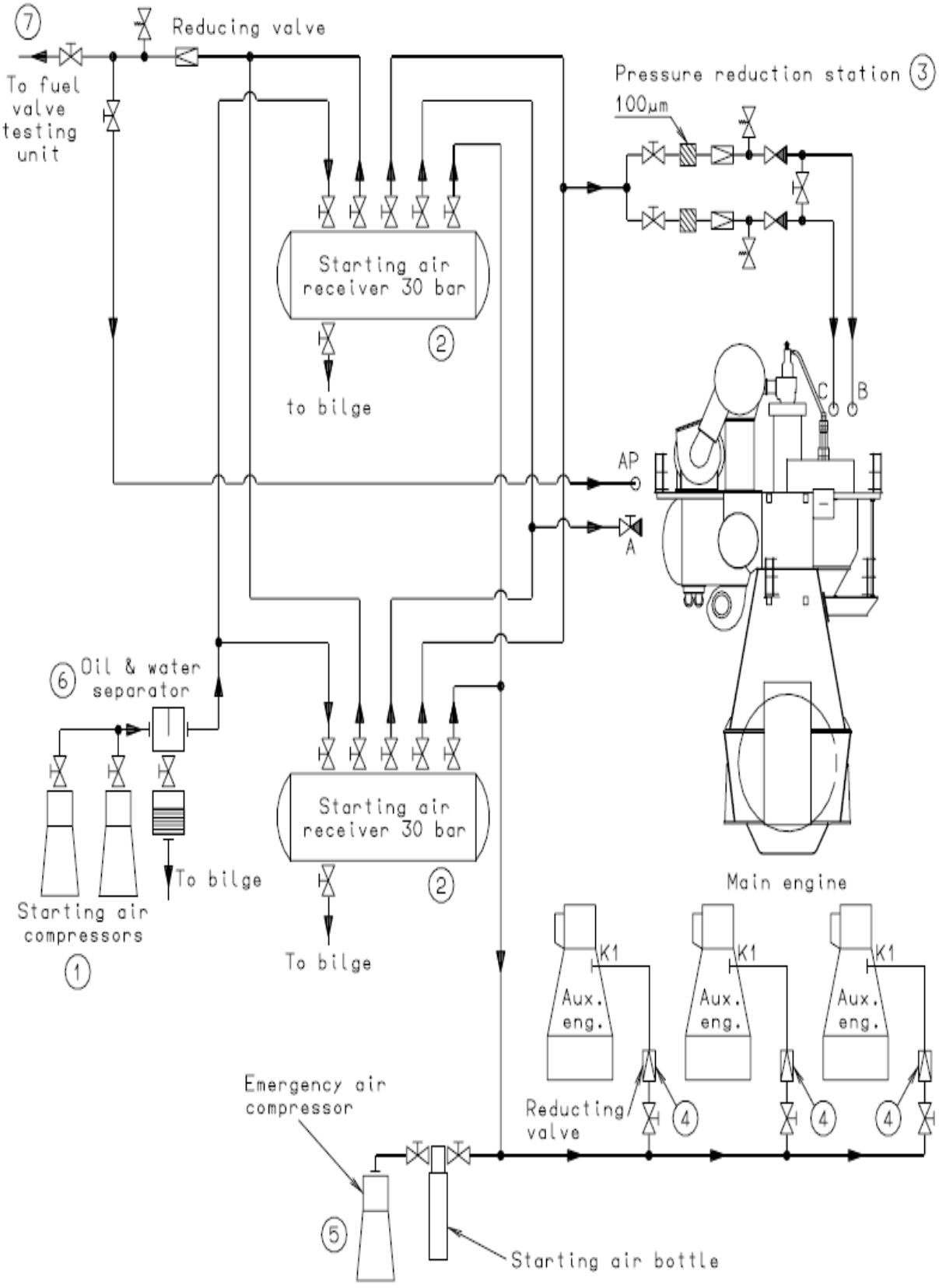

Figure 2.1: *Starting and Control Air Systems [2]*

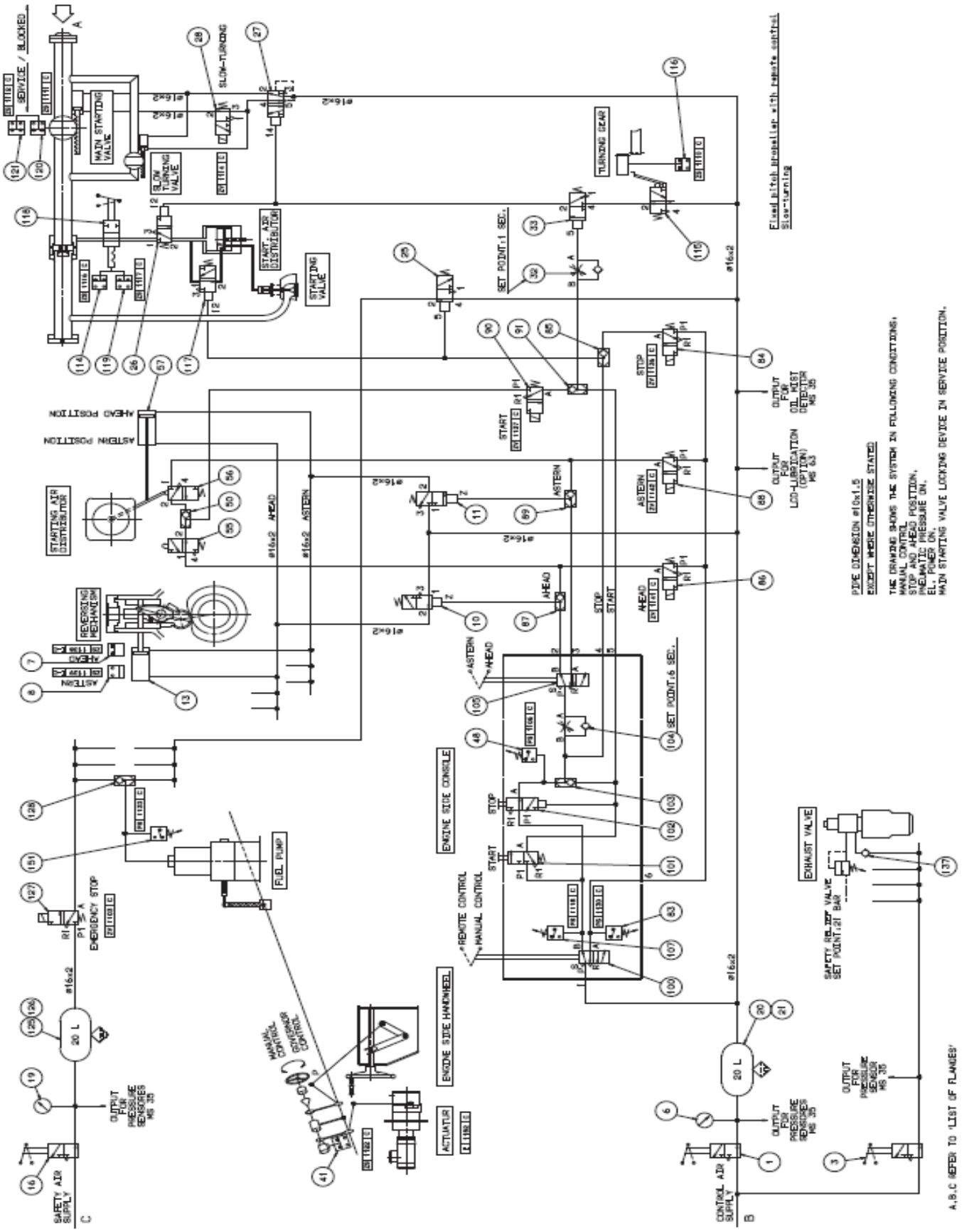

Figure 2.2: *Manoeuvring System Diagram [1]*

2.2 Starting Air System

The starting air system of a camshaft controlled two-stroke propulsion engine is incorporated into the manoeuvring system of the engine. The basic diagram of the manoeuvring system of a reversible engine, i.e. those directly connected with fixed pitch propellers, is shown in Figure 2.2.

The engine can be operated by three independent consoles, remotely from the bridge and the engine control room and locally from the engine side console. The manoeuvring diagram shows the basic engine control system that is used to start the engine, in the ahead or astern direction, to regulate its speed and to shut down the engine.

The starting air system of the engine, which is located at the upper right corner of the manoeuvring diagram (see Figure 2.2), is shown in Figure 2.3. The starting air system consists of three main components:

- the main starting valve
- the starting air distributor
- the starting valve

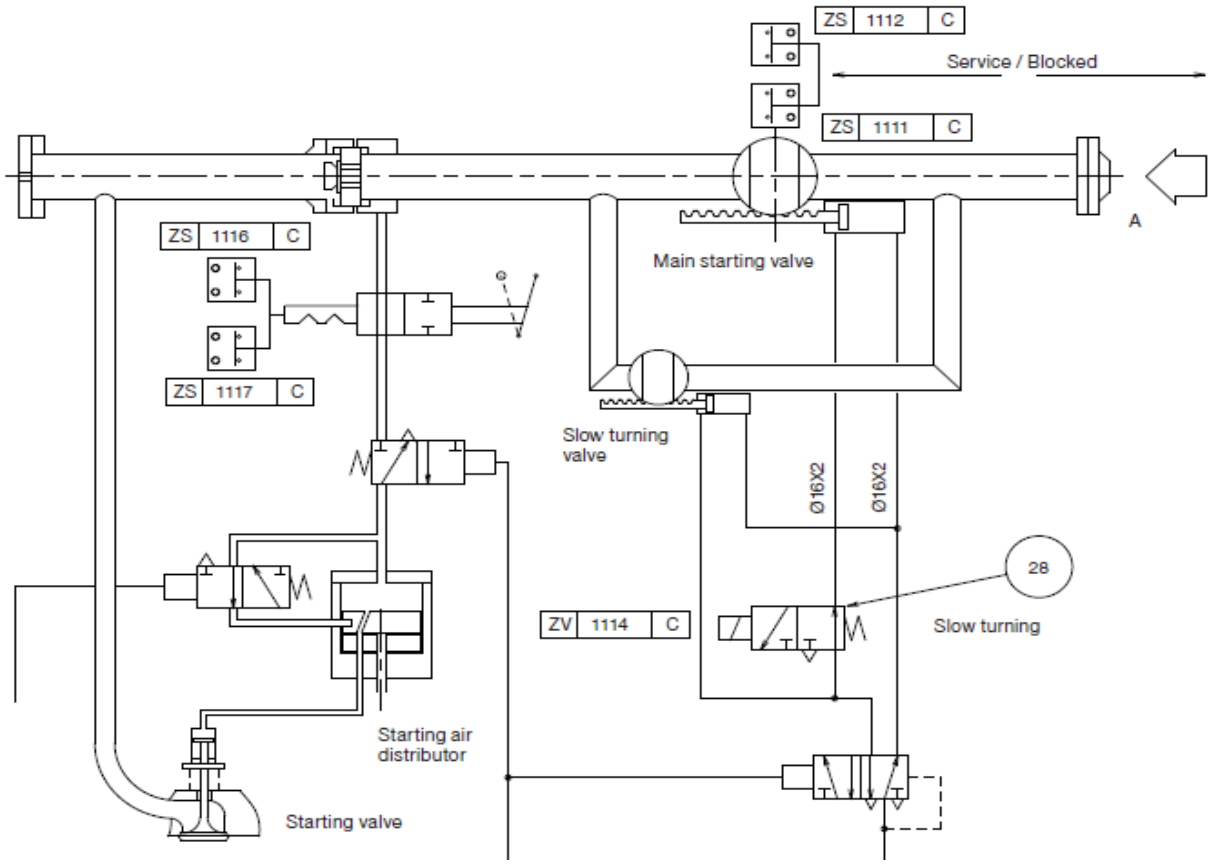

Figure 2.3: *Starting Air System [1]*

2.2.1 Main Starting valve

The main starting valve is operated by a pneumatic cylinder and is combined with the manoeuvring system, which controls the start of the engine. Its purpose is to isolate the starting valves from the starting air receivers during normal engine operation. A simple ball valve, actuated by a piston through a rack, is the most common design of a main starting valve.

The additional components required for slow turning are also shown in the starting air system of Figure 2.3. The slow turning function is optional and is actuated manually from the manoeuvring console [1]. The slow turning valve diverts the starting air to bypass the main starting valve. During slow turning, the engine rotates so slowly that, if liquids have accumulated on the piston top, the engine will stop before any harm occurs [1].

2.2.2 Starting Air Distributor

When the start command is given to the engine, control air is supplied to the starting air distributor according to the commanded starting direction, ahead or astern. In camshaft controlled engines, the starting air distributor is driven by the camshaft and its purpose is to regulate the supply of control air to the starting valves in accordance with the correct firing order. The starting air distributor can be basically of two kinds, the pilot valve and inverse cam type or the radial type.

Concerning the starting air distributor of the first type, the pilot valves are mounted axially, along with a set of inverse cams, for ahead and astern starting direction, respectively. A schematic diagram of an axial starting air distributor is shown in Figure 2.4. The pilot valve is a spool type pneumatic valve. The alternation of the starting air distributor's operation, between ahead and astern, is achieved by the axial shifting of the inverse cams using a pneumatic cylinder, as shown in Figure 2.2.

Large camshaft controlled diesel engines are usually equipped with the starting air distributor of the radial type. This type of starting air distributor has only one set of inverse cams and the pilot valves are mounted radially around this set of inverse cams. Depending on the commanded starting direction, the pilot valves are pushed by the control air to the inner or to the outer cam profile for ahead or reverse starting, respectively. A very descriptive sketch of the operation of a radial starting air distributor for ahead starting is shown in Figure 2.5, while in Figure 2.6 the same sketch shows its operation for the astern starting direction.

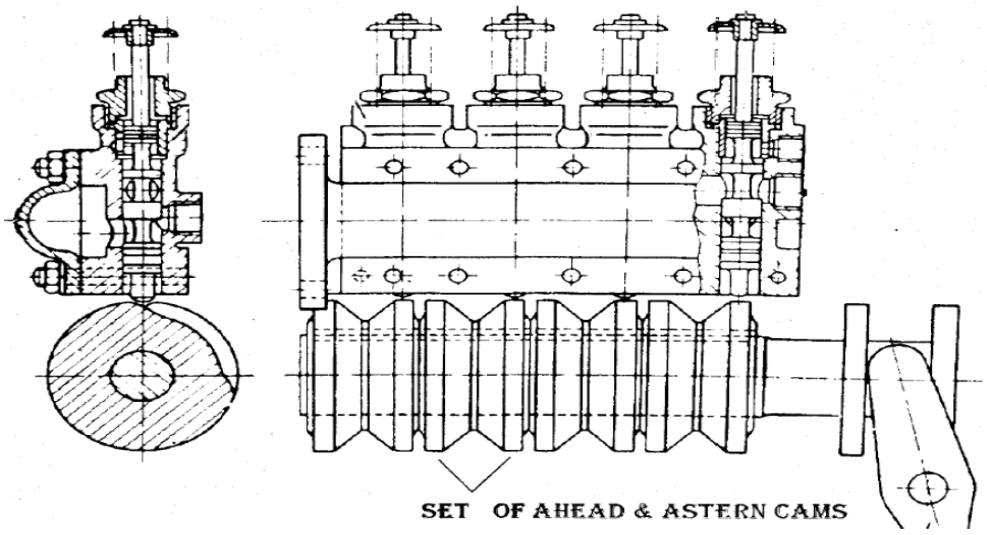

Figure 2.4: *Diagram of Axial Starting Air Distributor*

For both types of starting air distributors, each pilot valve operates one starting valve, so the number of pilot valves is equal to the number of cylinders. Engines that are fitted with radial starting air distributors and have more than nine cylinders require the installation of two starting air distributors.

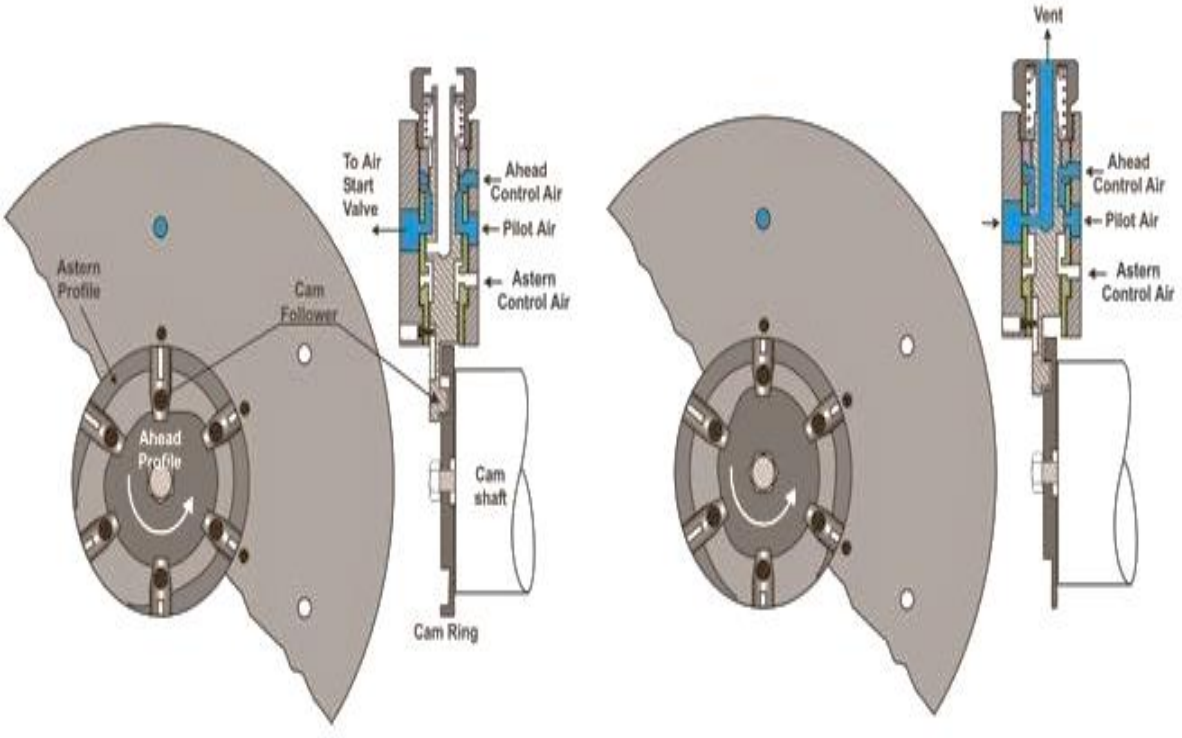

Figure 2.5: *Operation of Radial Starting Air Distributor for Ahead Starting*

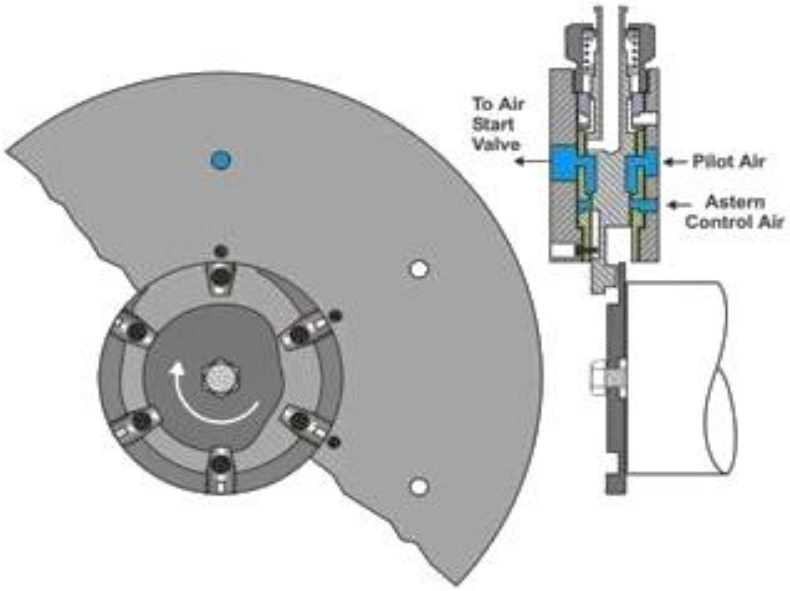

Figure 2.6: *Operation of Radial Starting Air Distributor for Astern Starting*

In most cases of air distributor designs, inverse cam geometry is preferred since it provides the easiest arrangement to disengage after the engine has successfully started. The pilot valves are pressed on the cams only during the stating procedure of the engine. During normal engine operation, control air pressure is not present and the cams turn freely. This way, reduced wear of the cams and the pilot valves is achieved. Lastly, this arrangement lowers the possibility of mistimed admission of compressed air into the cylinders due to stuck pilot valves or broken springs.

2.2.3 Starting Valve

As far as starting valves are concerned, one is fitted on each cylinder cap. They are operated by the starting air distributor and their purpose is to directly admit compressed air into the cylinder. They are designed in such a way that if the cylinder unit is firing, combustion pressure prevents the opening of the starting valve, even if the pneumatic pressure for opening is present. This design feature greatly reduces the chance of a starting air line explosion. The starting valves are opened pneumatically by control air from the starting air distributor(s) and are closed by a spring.

The compressed air is admitted into the cylinder during the expansion stroke, so as to produce positive torque. In two-stroke diesel engines, the starting valves open when the piston reaches the Top Dead Center (TDC) and close before the opening of the exhaust valve in uniflow scavenged engines, or the uncovering of exhaust ports in cross-flow or loop scavenged engines. In order to make full use of the compressed

air admission period, the cylinder should be fully pressurized right at TDC. If control air from the starting air distributor is sent when the piston reaches TDC, then, due to mechanical delay, the cylinder will be fully pressurized some degrees past TDC. Hence, the starting valves are timed to open just a few degrees before TDC to compensate for the mechanical delay. The usual timing of a starting valve, when the engine is operating in the ahead direction, is shown in Figure 2.7.

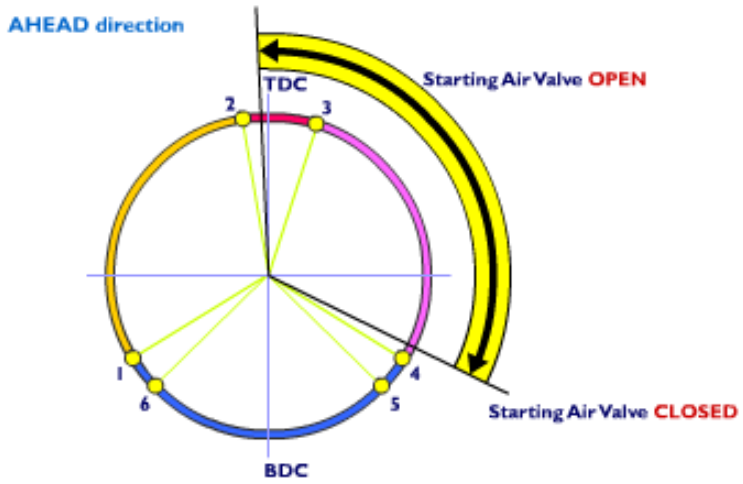

Figure 2.7: *Starting Valve Timing for Engine Operation in the Ahead Direction*

The engine is to be able to start from any initial crank position. The timing of the starting valves ensures that at least one valve will open to accelerate the engine in the appropriate direction, irrespective of the initial crank position. This is known as the overlapping period.

2.3 Starting and Reversing the Engine

The starting air system described in the previous section produces sufficient torque to accelerate the engine to the speed required for ignition. When the engine reaches the required level of crankshaft revolutions, the governor sets the fuel pump index to the corresponding starting fuel dosage. Then, fuel is injected into the cylinders and the engine starts its normal operation. The level of crankshaft revolutions for initial fuel injection is in the range of 8 to 12% of the engine's revolutions at Maximum Continuous Rating (MCR) (see Figure 2.10).

If the engine is to be started in the reverse direction, then the engine's firing order has to be reversed. Engine operation in the reverse direction can be better understood by considering the processes during a cylinder cycle. Any process that is not symmetrically timed around TDC or Bottom Dead Center (BDC) has to be reversed. The inlet ports, for instance, are symmetrically timed around BDC and

don’t need to be reversed. The exhaust valve is not to be reversed, as well [1]. Nevertheless, the fuel injection timing and the timing of the starting valves have to be reversed.

The reversal of the timing of the starting valve is achieved by alternating the starting air distributor’s cams accordingly, as described in Section 2.2.3, while the reversal of fuel injection timing is performed by means of an angular shift of the displaceable roller in the driving mechanism of the fuel pump. The reversing mechanism is operated by a pneumatic cylinder and is shown in Figure 2.8.

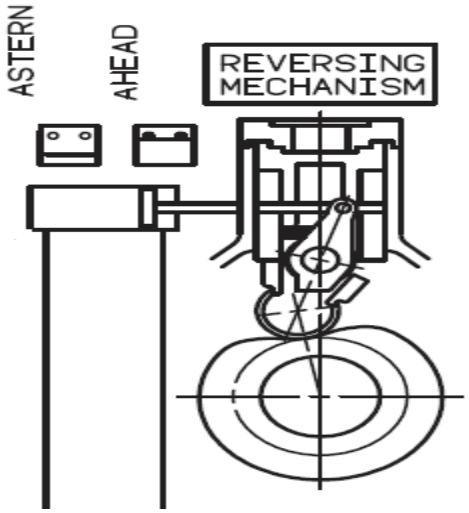

Figure 2.8: *Fuel Pump Reversing Mechanism [1]*

The timing of a starting valve, when the engine is operating in the astern direction, is shown in Figure 2.9.

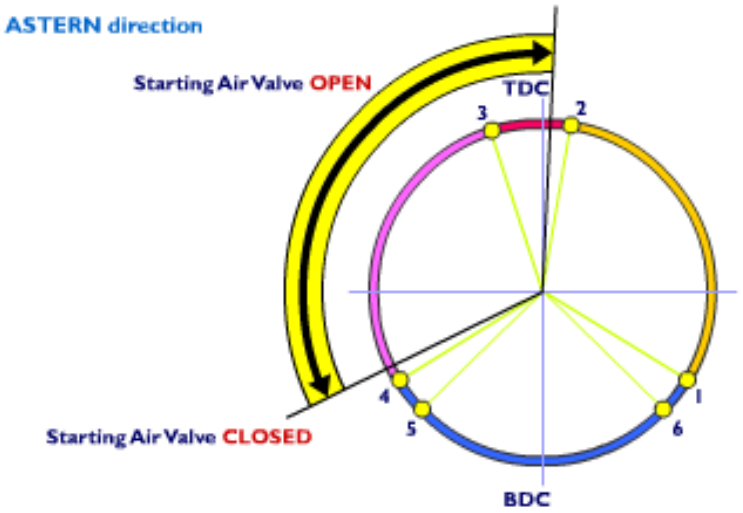

Figure 2.9: *Starting Valve Timing for Engine Operation in the Astern Direction*

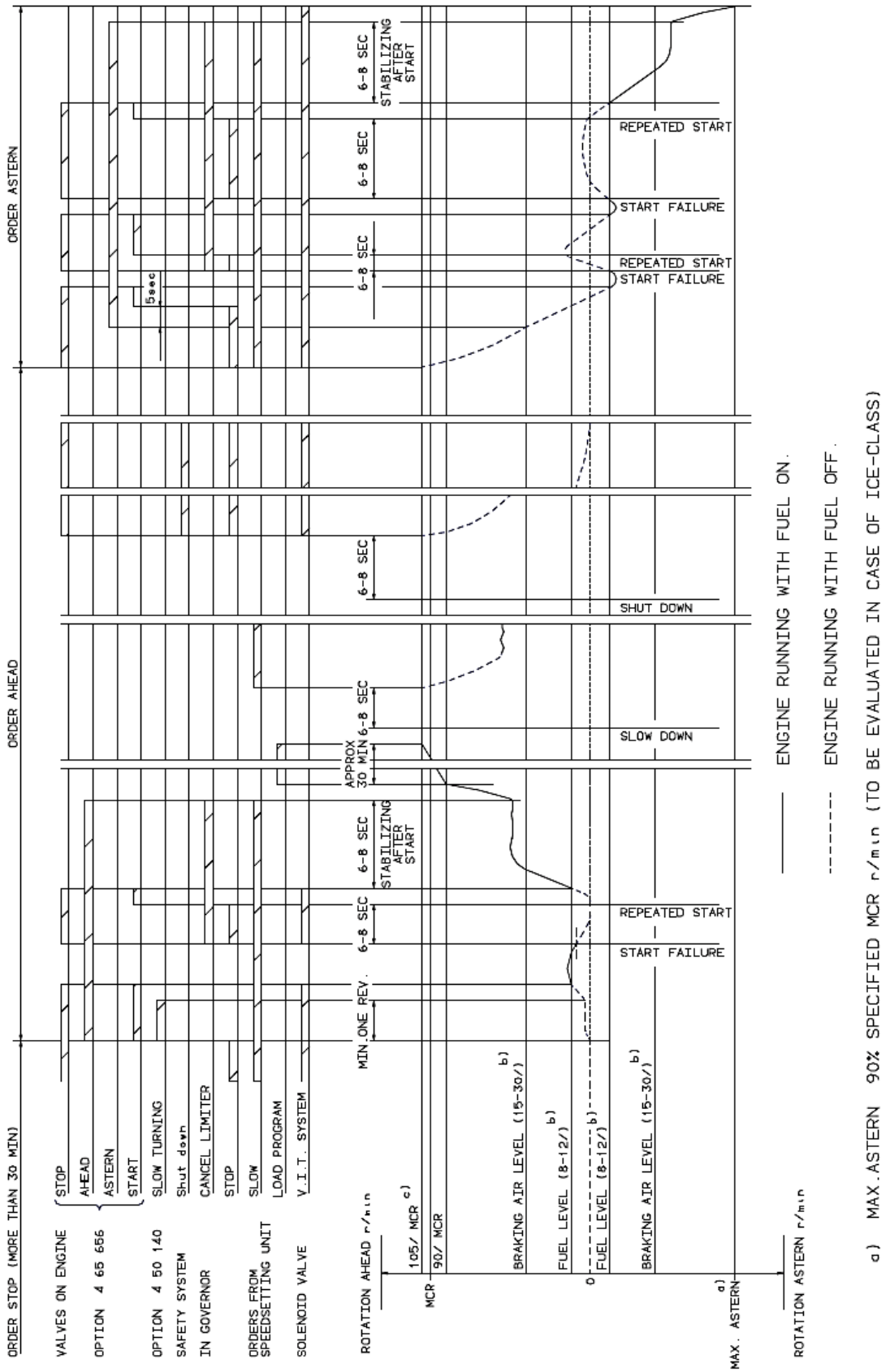

Figure 2.10: *Sequence Diagram of Reversible Engines [1]*

During the crash-stop manoeuvre of a ship, the engine has to be braked while it is still running in the ahead direction and then started in the opposite direction. After the fuel supply to the engine is cut off, the engine decelerates until it reaches the braking air level of crankshaft revolutions. Compressed air can then be admitted directly into the cylinders, in the astern direction timing, in order to brake the engine. The level of crankshaft revolutions, for braking air to be safely admitted, is in the range of 15 to 30% of the engine's revolutions at MCR, as shown in Figure 2.10. Finally, the engine can be started in the astern direction and accelerated to the maximum permissible astern revolutions which is approximately 90% of the engine's revolutions at MCR (see Figure 2.10).

2.4 Scavenge Air System - Auxiliary Blowers

Large uniflow scavenged diesel engines are fitted with at least one turbocharger, located on the exhaust side of the engine, to supply the engine with the required amount of scavenge air. The compressor draws air from the engine room through an air filter and then compresses it. The compressed air is cooled by the scavenge air cooler, so as to decrease its density. The scavenge air system is an integrated part of the main engine and is shown in Figure 2.11.

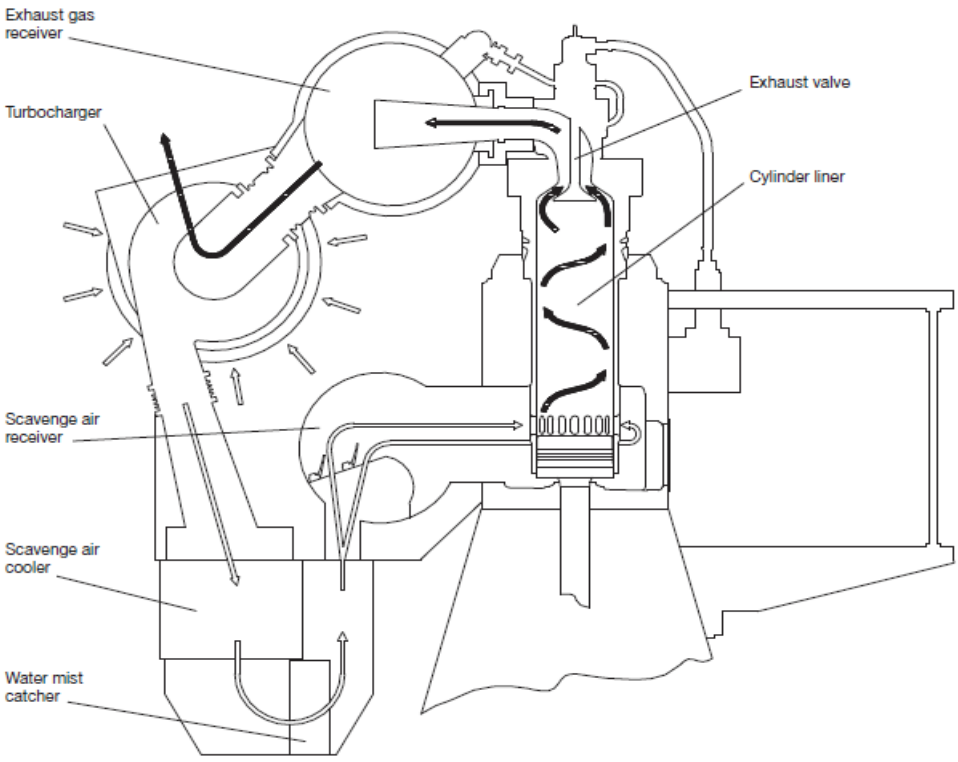

Figure 2.11: *Diagram of the Scavenge Air System [1]*

Large two-stroke diesel engines are also equipped with at least two auxiliary blowers, driven by electric motors. The actual number of auxiliary blowers depends on the number of cylinders as well as the turbocharger make and amount [1].The auxiliary blowers are installed between the scavenge air cooler and the scavenge air receiver. Non-return valves, which close automatically when the auxiliary blowers are operating, are also fitted.

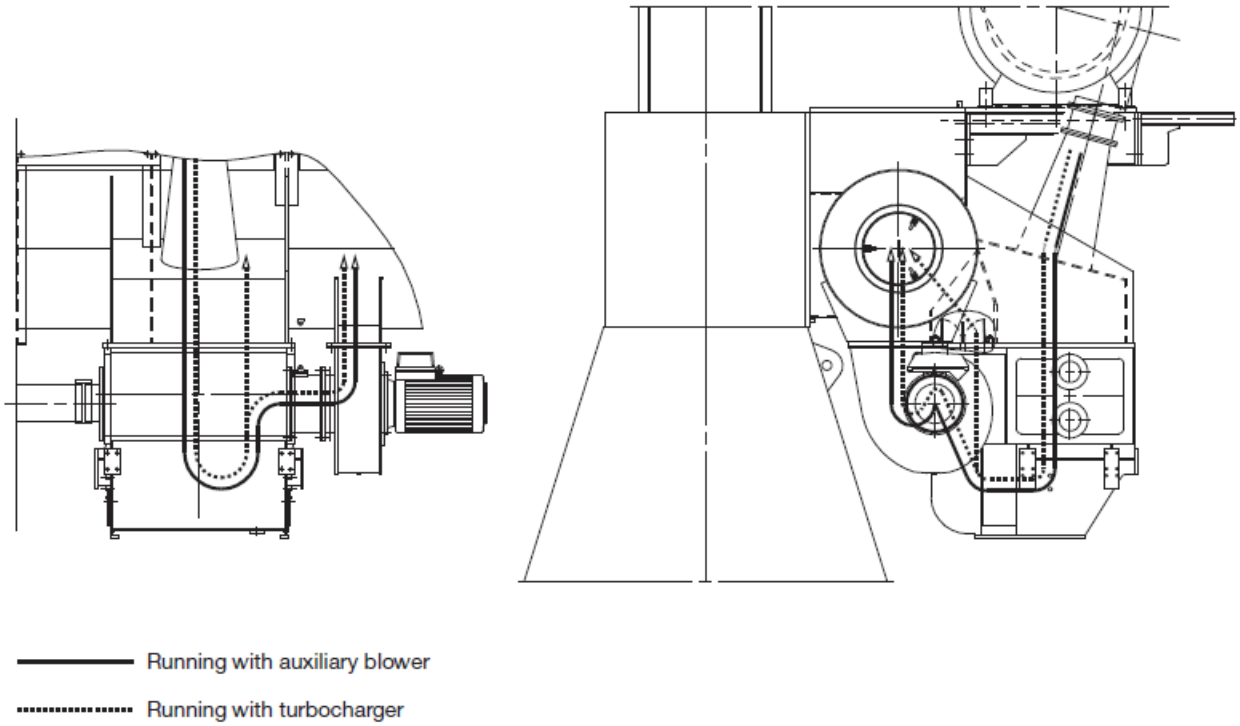

Figure 2.12: *Operation of the Auxiliary Blowers [1]*

Before the engine is started, the auxiliary blowers start operating to ensure complete scavenging of the cylinders during the starting phase, thus providing the best conditions for a safe start [1]. During normal engine operation, the auxiliary blowers will start automatically whenever the scavenge pressure drops below a critical value and will shut down when adequate scavenge air pressure is present.

2.5 Regulatory Framework

All the regulations concerning the starting air system of propulsion engines is published as part of the Unified Requirements (UR) of the International Association of Classification Societies (IACS). Unified Requirements are the minimum requirements and each member of the IACS remains free to set more strict requirements.

The intent of the requirements for the starting air system is to provide propulsion engines with ready and adequate supply, as well as an adequate reserve, of starting air and to provide for proper design and protection of the compressed air system.

For the starting arrangement of a representative propulsion engine, at least two starting air receivers of approximately the same size are to be installed. The total capacity of the air receivers is to be sufficient to provide, without being replenished, at least twelve consecutive starts, alternating between ahead and astern direction, for each main engine of the reversible type, or at least six consecutive starts for each main engine of the non-reversible type. If the compressed air is used for other purposes as well, the total capacity of the air receivers should be increased accordingly.

As far as the air compressors are concerned, at least two are to be installed and at least one should be driven independently of the propulsion engine. The total capacity of the air compressors is to be sufficient to supply, within one hour, the quantity of air needed to fully charge the air receivers from atmospheric pressure. Lastly, the total capacity of the air compressors driven independently of the main engine shouldn't be less than 50% of the total required.

For ships with multi-engine installations, or non-conventional propulsion systems, the number of starts required for each engine may be calculated upon the agreement with the Classification Society. For instance, American Bureau of Shipping (ABS) states that the minimum number of consecutive starts required to be provided from the starting air receivers, for diesel or turbine propulsion systems, is to be based upon the arrangement of the engine(s) and shafting system(s), as indicated in the following Table 2.1.

	Single Propeller Vessels		Multiple Propeller Vessels	
Engine Type	One engine coupled to shaft directly or through reduction gear	Two or more engines coupled to shaft through clutch and reduction gear	One engine coupled to each shaft directly or through reduction gear	Two or more engines coupled to each shaft through clutch and reduction gear
Reversible	12	16	16	16
Non-Reversible	6	8	8	8

Table 2.1: *Required Number of Starts for Propulsion Engine(s) [3]*

Concerning diesel-electric or turbine-electric propulsion, the minimum number of consecutive starts required to be provided from the starting air receivers, is to be determined from the following equation:

$$S = 6 + G \cdot (G - 1) \qquad (2.5.1)$$

where S is the total number of consecutive starts and

G is the number of engines necessary to maintain sufficient electrical load to permit vessel transit at full seagoing power and manoeuvring, but should not exceed 3

3 Engine Model

3.1 Introduction

Two main types of engine models can be used for the simulation of the transient behavior of the marine diesel engine, the mean value models and the phenomenological models. The mean value models, which are quite simplified, are mainly used for design purposes of engine control systems. The phenomenological models can be of the control volume type, also known as zero-dimensional models, but can also incorporate one-dimensional calculations in order to more accurately represent flow processes and phenomena [4]. This type of engine simulation models are more detailed and require larger amount of input data, hence, they are more appropriate to predict the performance of a large marine two-stroke diesel engine under transient conditions.

The objective of the present thesis is the prediction of the engine's transient response during its starting phase. Thus, a model of the second type is used for the accurate prediction of the engine performance. In that respect, the MOtor THERmodynamics (MOTHER) engine simulation code is used.

MOTHER is an engine simulation and performance prediction code which falls under the category of zero-dimensional or control volume engine simulation models. It considers the engine as a sequence of interconnected volumes via valves or ports, assuming spatial uniformity of fluid properties and constant rate of change of parameters in each control volume at any computational time step [5]. The MOTHER engine simulation code has been under development for a number of years in the Laboratory of Marine Engineering and is capable of predicting the engine and turbocharger performance under transient conditions.

The present Chapter describes the basic governing equations of the thermodynamic and mechanical elements that are being used to model the engine configuration. A much more detailed description of the models used can be found in [5].

3.2 Marine Diesel Engine Model

As was mentioned, the MOTHER engine simulation and performance prediction code is of the control volume (filling and emptying) type. The basic elements that are

used to form the engine structure are the control volumes (Flow Receivers), such as the cylinders and plenums of any type, interconnected via valves or ports (Flow Controllers). For the transfer of mechanical work a crankshaft and other shafts (Mechanical Elements) are used. Lastly, the engine environment is regarded as a fixed fluid element with constant temperature, pressure and composition.

3.2.1 Flow Receivers

The flow receivers are modeled as open thermodynamic systems where work, heat and mass transfer take place through their boundaries. In order to derive the equations describing the processes that take place in the control volumes, the following general assumptions are made [5]:

- thermodynamic equilibrium and perfect gas behavior for the working medium
- spatial uniformity of fluid properties at each instant
- potential energy variations are neglected
- quasi-steady and one-dimensional flow through valves and ports at each instant
- pressure wave interactions are ignored

The state of the working medium at any instant is described by its temperature, pressure and equivalence ratio, i.e.:

$$u = u(T,\ p,\ \varphi) \tag{3.2.1}$$

$$R = R(T,\ p,\ \varphi) \tag{3.2.2}$$

Three main laws are used to describe the processes taking place inside each flow receiver and calculate the properties of the working medium at any instant:

- the energy conservation law
- the mass conservation law
- the perfect gas law

The first law of thermodynamics (energy conservation) for an open thermodynamic system, neglecting potential energy terms, can be written in the following general form:

$$\frac{dU}{dt} = \frac{dQ}{dt} - \frac{dW}{dt} + \sum_j \frac{dH_{0j}}{dt} \tag{3.2.3}$$

or

$$\frac{d(m\cdot u)}{dt}=\sum_{j}\frac{dQ_{sf}}{dt}-p\cdot\frac{dV}{dt}+\sum_{j}h_{oj}\frac{dm_{j}}{dt} \tag{3.2.4}$$

Assuming homogeneous formulation of the working medium and differentiating the left-hand side of equation (3.2.4), the following equation is derived:

$$m\cdot\frac{du}{dt}+u\cdot\frac{dm}{dt}=\sum_{j}\frac{dQ_{sf}}{dt}-p\cdot\frac{dV}{dt}+\sum_{j}h_{oj}\frac{dm_{j}}{dt} \tag{3.2.5}$$

The rate of change of the internal energy of the working medium can be derived from the equation (3.2.1):

$$\frac{du}{dt}=\frac{\partial u}{\partial T}\cdot\frac{dT}{dt}+\frac{\partial u}{\partial p}\cdot\frac{dp}{dt}+\frac{\partial u}{\partial R}\cdot\frac{dR}{dt} \tag{3.2.6}$$

Substituting equation (3.2.6) into equation (3.2.5), the energy conservation law can be written:

$$m\cdot\left(\frac{\partial u}{\partial T}\cdot\frac{dT}{dt}+\frac{\partial u}{\partial p}\cdot\frac{dp}{dt}+\frac{\partial u}{\partial R}\cdot\frac{dR}{dt}\right)+u\cdot\frac{dm}{dt}=\sum_{sf}\frac{dQ_{sf}}{dt}-p\cdot\frac{dV}{dt}+\sum_{j}h_{oj}\frac{dm_{j}}{dt} \tag{3.2.7}$$

Exploiting the assumption for perfect gas behavior of the working medium we can use the perfect gas law to derive an equation for the calculation of the pressure and the pressure rate of change for the working medium:

$$p\cdot V=m\cdot R\cdot T\Rightarrow p=\frac{m\cdot R\cdot T}{V} \tag{3.2.8}$$

$$\frac{dp}{dt}=\frac{\frac{dT}{dt}\cdot\left(\frac{1}{T}+\frac{1}{R}\cdot\frac{\partial R}{\partial T}\right)+\frac{1}{R}\cdot\frac{\partial R}{\partial\varphi}\cdot\frac{d\varphi}{dt}+\frac{1}{m}\cdot\frac{dm}{dt}-\frac{1}{V}\cdot\frac{dV}{dt}}{1-\frac{p}{R}\cdot\frac{\partial R}{\partial p}}\cdot p \tag{3.2.9}$$

Substituting equations (3.2.8) and (3.2.9) into equation (3.2.7), the temperature rate of change for the working medium can be written:

$$\frac{dT}{dt}=\frac{B-\frac{\partial u}{\partial\varphi}\cdot\frac{d\varphi}{dt}-\frac{p}{D}\cdot\frac{\partial u}{\partial p}\cdot\left(\frac{1}{R}\cdot\frac{\partial R}{\partial\varphi}\cdot\frac{d\varphi}{dt}+\frac{1}{m}\cdot\frac{dm}{dt}-\frac{1}{V}\cdot\frac{dV}{dt}\right)}{\frac{\partial u}{\partial T}+\frac{\partial u}{\partial p}\cdot\frac{p}{T}\cdot\frac{C}{D}} \tag{3.2.10}$$

where

$$B = \frac{1}{m} \cdot \left(\sum_j \frac{dQ_{sf}}{dt} - u \cdot \frac{dm}{dt} + \sum_j h_{oj} \frac{dm_j}{dt} \right) - \frac{R \cdot T}{V} \cdot \frac{dV}{dt}$$

$$C = 1 + \frac{T}{R} \cdot \frac{\partial R}{\partial T}$$

$$D = 1 - \frac{p}{R} \cdot \frac{\partial R}{\partial p}$$

Equation (3.2.10) is the basic form of the energy conservation law that is used in each control volume, together with the mass conservation law:

$$\frac{dm}{dt} = \sum_j \frac{dm_j}{dt} \tag{3.2.11}$$

The calculation of equation (3.2.10) requires the calculation of some terms on the right-hand side of the equation, such as the volume and the equivalence ratio rates of change. While the volume rate of change of engine plenums, such as the scavenge receiver and the exhaust receiver is zero, the volume rate of change of each cylinder can be expressed as a function of cylinder geometry, crank angle and crankshaft angular velocity:

$$\frac{dV}{dt} = \frac{\pi \cdot B^2}{4} \cdot \left[r \cdot \sin\theta \cdot \frac{d\theta}{dt} + \left(1 - r^2 \cdot \sin^2\theta\right)^{-1/2} \cdot r^2 \cdot \sin\theta \cdot \cos\theta \cdot \frac{d\theta}{dt} \right] \tag{3.2.12}$$

The rate of change of the gas equivalence ratio in a flow receiver can be expressed as a function of the fuel injection rate, the burnt fuel mass flow rate and the combustion products entering or exiting the flow receiver, and is given by the following equation:

$$\frac{d\varphi}{dt} = \frac{F_1}{m} \cdot \left(\frac{F_1}{f_s} \cdot \frac{dm_{fb}}{dt} - \varphi \cdot \frac{dm}{dt} \right) \tag{3.2.13}$$

where

$$F_1 = 1 + \varphi \cdot f_s \tag{3.2.14}$$

$$\frac{dm_{fb}}{dt} = \sum_j \left(\frac{m_{fb,j}}{m_j} \cdot \frac{dm_j}{dt} \right)_{inlet} - \sum_j \left(\frac{m_{fb,j}}{m_j} \cdot \frac{dm_j}{dt} \right)_{outlet} + \frac{dm_f}{dt} \tag{3.2.15}$$

Some final remarks on some engine sub-models should be discussed. Concerning cylinders, combustion is modeled as a heat release process using cumulative fuel burning rate diagrams (S-curve functions). The heat transfer, for any flow receiver element is modeled as a two part process, heat transfer between the

working medium and the element wall and heat transfer between the wall and the coolant.

3.2.2 Flow Controllers

As was previously mentioned, the flow receiver elements are interconnected via flow controller elements (valves or ports). The mass flow rates through the latter are required in order to calculate the energy conservation equation (3.2.10). The main flow controllers are the scavenge ports connecting the cylinder with the scavenge receiver and the exhaust valve connecting the cylinder with the exhaust receiver.

The flow controllers are modeled using a simple one-dimensional quasi-steady orifice flow model. The model is derived by applying the energy equation from upstream to the valve throat, assuming isentropic steady flow [5].

If the flow controller's pressure ratio upstream to downstream is below the critical value $\left(\frac{p_u}{p_d}\right) < p_{cr} = \left(\frac{\gamma+1}{2}\right)^{\frac{\gamma}{\gamma-1}}$, then the flow is subsonic and the mass flow rate can be written:

$$\frac{dm_j}{dt} = A_e \cdot p_u \cdot \sqrt{\frac{2\cdot\gamma}{\gamma-1}\cdot\frac{1}{R\cdot T_u}\cdot\left[\left(\frac{p_d}{p_u}\right)^{\frac{2}{\gamma}} - \left(\frac{p_d}{p_u}\right)^{\frac{\gamma+1}{\gamma}}\right]} \qquad (3.2.16)$$

where $\gamma = c_p / c_v$ is the specific heat ratio.

Otherwise, if the pressure ratio is sufficient to choke the flow through the valve, $\left(\frac{p_u}{p_d}\right) \geq p_{cr}$, the mass flow rate equation becomes:

$$\frac{dm_j}{dt} = A_e \cdot p_u \cdot \sqrt{\frac{\gamma}{R\cdot T_u}\cdot\left(\frac{2}{\gamma+1}\right)^{\frac{\gamma+1}{\gamma-1}}} \qquad (3.2.17)$$

3.2.3 Mechanical Elements

Mechanical elements are used to model the power transfer between rotating masses, connected by perfectly rigid shafts. The instantaneous angular acceleration of any shaft can be calculated by applying the momentum equation:

$$\frac{d\omega}{dt} = \frac{\sum_i \tau_i}{I_{tot}} \tag{3.2.18}$$

The numerator consists of the sum of all the torque values exerted on the shaft or absorbed by a load, while the denominator comprises the polar moment of inertia of every rotating mass attached to the shaft.

Such elements are used to model both the engine crankshaft and the turboshaft. Cylinders are considered to be mechanically connected to the crankshaft, along with the propeller. The cylinders produce torque, whereas the propeller absorbs torque. The turbine and the compressor are connected to the turboshaft and the turbine produces torque, whereas the compressor absorbs torque.

4 Starting System Model

The starting system configuration of large two-stroke propulsion engines was described in the second Chapter. The main components of the starting air system will be modeled using the basic thermodynamic elements of the MOTHER engine simulation and performance prediction code. Starting air receivers will be modeled as flow receivers and starting valves as flow controllers. The working medium of these elements is the air, something that leads to major simplifications and the equations describing the thermodynamic elements will be modified accordingly. Lastly, a friction torque model, incorporating the friction characteristics during the starting phase of the engine, is presented.

4.1 Starting Air Receivers

The starting air receivers are modeled as plenums charged with compressed air, using a flow receiver element. The volume of the plenum and the equivalence ratio of the working medium are constant. Hence, the rate of change of these two properties will be equal to zero, i.e. $dV/dt = 0$ and $d\varphi/dt = 0$, respectively. Moreover, the equivalence ratio of the working medium is considered to be equal to zero.

The equations describing the instantaneous state of the gas inside the starting air receiver can be calculated as a function of its temperature and pressure. Thus, equations (3.2.1) and (3.2.2) can be written:

$$u = u(T,\ p,\ \varphi = 0) \Rightarrow u = u(T,\ p) \tag{4.1.1}$$

$$R = R(T,\ p,\ \varphi = 0) \Rightarrow R = R(T,\ p) \tag{4.1.2}$$

Another major simplification is derived from the assumption that the compressed air is discharged from the starting air receiver adiabatically, i.e. $dQ_{sf}/dt = 0$, because it is very difficult to calculate a heat transfer coefficient. Moreover, the discharging process lasts for just a few seconds and previous studies on the discharging of air vessels showed acceptable results compared to experimental data, using the same adiabatic assumption.

Keeping in mind all the aforementioned simplifications, equation (3.2.10), which is used to calculate the temperature rate of change, can be rewritten:

$$\frac{dT}{dt} = \frac{B - \frac{p}{D} \cdot \frac{\partial u}{\partial p} \cdot \frac{1}{m} \cdot \frac{dm}{dt}}{\frac{\partial u}{\partial T} + \frac{\partial u}{\partial p} \cdot \frac{p}{T} \cdot \frac{C}{D}} \tag{4.1.3}$$

where

$$B = \frac{1}{m} \cdot \left(-u \cdot \frac{dm}{dt} + \sum_j h_{oj} \frac{dm_j}{dt} \right)$$

$$C = 1 + \frac{T}{R} \cdot \frac{\partial R}{\partial T}$$

$$D = 1 - \frac{p}{R} \cdot \frac{\partial R}{\partial p}$$

Lastly, the pressure drop of the starting air receiver at any instant is calculated in reference to equation (3.2.9), using the following equation:

$$\frac{dp}{dt} = \frac{\frac{dT}{dt} \cdot \left(1 + \frac{T}{R} \cdot \frac{\partial R}{\partial T} \right) + \frac{1}{m} \cdot \frac{dm}{dt}}{1 - \frac{p}{R} \cdot \frac{\partial R}{\partial p}} \cdot p \tag{4.1.4}$$

4.2 Starting Valve

The starting valves are modeled using Flow Controller elements and connect the cylinders to the starting air receivers. The mass flow rate through the starting valves is calculated using equation (3.2.16) or equation (3.2.17), as a function of the upstream to downstream pressure ratio, and can be written explicitly for air being the working medium, i.e. $\gamma = 1.4$.

If the starting valve's pressure ratio upstream to downstream is below the critical value $\left(\frac{p_u}{p_d} \right) < p_{cr} = \left(\frac{\gamma + 1}{2} \right)^{\frac{\gamma}{\gamma - 1}} \simeq 1.893$, then the flow is subsonic and the mass flow rate equation is written:

$$\frac{dm_j}{dt} = A_e \cdot p_u \cdot \sqrt{\frac{7}{R \cdot T_u} \cdot \left[\left(\frac{p_d}{p_u} \right)^{1.4286} - \left(\frac{p_d}{p_u} \right)^{1.7143} \right]} \tag{4.2.1}$$

Otherwise, if the pressure ratio is sufficient to choke the air flow through the starting valve, $\left(\frac{p_u}{p_d}\right) \geq p_{cr} \simeq 1.893$, the mass flow rate equation becomes:

$$\frac{dm_j}{dt} = A_e \cdot p_u \cdot \sqrt{\frac{0.4689}{R \cdot T_u}} \tag{4.2.2}$$

Lastly, the flow through the starting valve is considered to be adiabatic, so the total enthalpy of air upstream and downstream remains constant, i.e. $h_{ou} = h_{od}$.

4.3 Friction Model

In most cases of engine friction modeling, the total engine frictional losses are expressed in terms of friction mean effective pressure. The friction mean effective pressure, in most models, such as the ones of McAuly et al., Winterbone and Tennant and Millington and Hartles [5], is expressed as a function of cylinder peak pressure, mean piston speed and engine rotational speed involving many coefficients. These models are proven quite adequate for modeling steady state conditions but in the present thesis another approach was followed.

In the present thesis the frictional losses were modeled as an external torque load connected to the engine crankshaft. The friction torque is expressed as a function of shaft speed, trying to incorporate the frictional losses of the whole ship shafting system. In such a complicated system, as the shafting system of a propulsion installation, many individual components contribute to the total frictional losses, making it almost impossible not to approach them as a whole. The main components contributing are the crankshaft bearings, the thrust bearing, the intermediate and propeller shaft bearings, the piston rings and crosshead bearings.

Moreover, during the starting phase of the engine, its initial speed is equal to zero and gradually increases, so friction mechanics for low velocities should be taken into account. The basics of friction mechanics as a function of velocity, for low velocities, will be discussed, in reference to Figure 4.1.

There are four main regions describing friction mechanics in systems with grease or oil lubrication. The static friction, boundary lubrication, partial fluid lubrication and full lubrication region. The static friction (sticktion) is the torque necessary to initiate motion from rest. In order to achieve break-away, the transition from rest to motion, the required amount of torque has to be exerted (break-away torque). In the second region, fluid lubrication is not important because the velocity is not

adequate to build a fluid film between the surfaces. The boundary layer might be considered solid, but due to lower shear strength, the friction is usually reduced. The third region describes the transition from boundary lubrication to full fluid lubrication. The friction behavior in this region is often termed as the Stribeck effect, during which, decreased friction is observed with increasing velocity. As the velocity increases the fluid film is getting thicker and when it becomes sufficiently thick the load is fully supported by the fluid film. Lastly, in the fourth region full fluid lubrication is present and the friction is a function of surface geometry, lubricant viscosity and velocity [6].

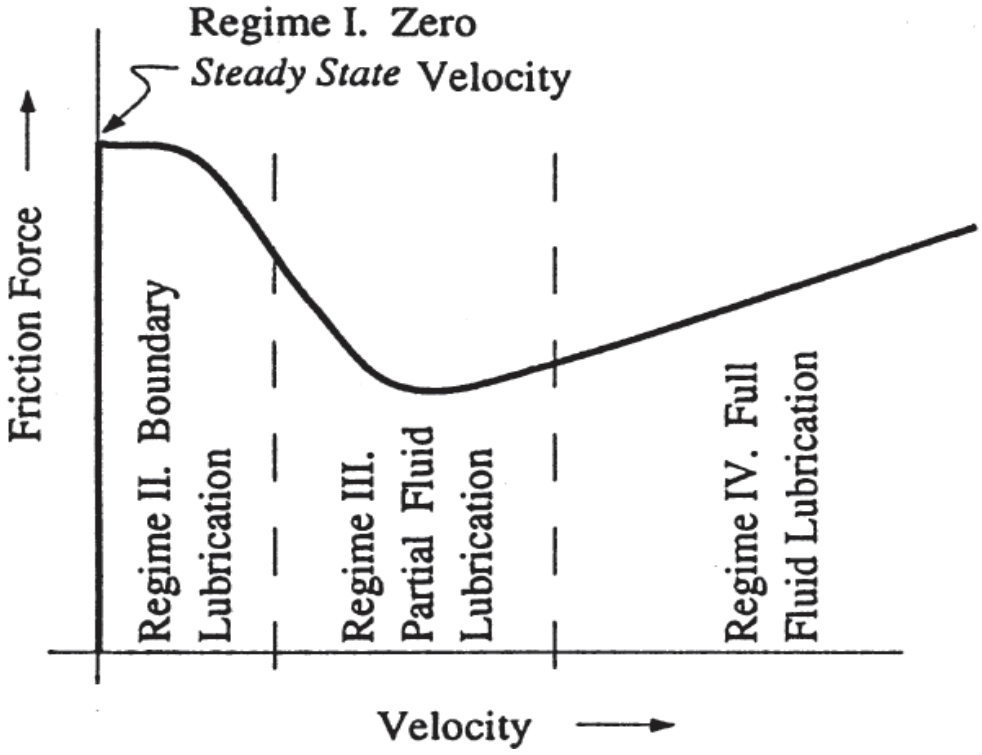

Figure 4.1: *Friction as a function of Velocity for Low Velocities [6]*

As was mentioned, due to the complexity of the shafting system and the lack of experimental data concerning friction at low velocities for large two-stroke diesel engines, a simplified model for the calculation of friction torque is introduced. The friction torque is expressed as a function of the engine speed, the shafting system break-away (static) torque and the frictional losses of the engine under steady state loading conditions. The friction torque can be calculated at any instant using the following equation:

$$Q_{fr} = Q_{st} + \frac{Q_{fr,100\%} - Q_{st}}{N_{MCR}} \cdot N \qquad (4.3.1)$$

The friction torque at 100% engine load was derived from simulations corresponding to steady state loading conditions. As far as the static friction torque is concerned, it was derived from the maximum torque of the engine's turning gear electric motor. The turning gear is mounted on the bedplate and is driven by an electric motor. It is used to drive the turning wheel which is fitted to the thrust shaft. Using the turning gear, the engine can be rotated at a very low rate, below one revolution per minute, for inspection purposes.

5 Turbocharger Modeling

All current large marine engines are turbocharged. Turbochargers consist basically of a turbine and a compressor connected in a common shaft. The power produced by the expansion of the exhaust gas in the turbine is used to drive the compressor [4]. An air cooler is installed after each compressor to reduce the density of the compressed air. In addition, usually two auxiliary air blowers are fitted to ensure sufficient cylinder scavenging at low load engine operation.

Under transient loading conditions, the response of the turbocharged marine diesel engines is limited by the turbocharger behavior. During acceleration, it takes time for pressure to be increased in the exhaust and scavenge receiver. Furthermore, part of the turbine power is spent to accelerate the turboshaft. Thus, the engine boost pressure will be lower than the one corresponding to steady state conditions. On the other hand, during fast deceleration fuel is reduced immediately, but due to the inertia of the turbocharger's rotating parts, the compressor pressure ratio is greater than the one corresponding to steady state conditions. Under such conditions, the compressor operation might become unstable.

5.1 Compressor Modeling

The performance of a compressor is usually modeled using performance maps obtained experimentally by the manufacturer under steady state conditions. The performance maps consist of constant speed curves relating the mass flow rate passing through the compressor with the compressor pressure ratio. Each constant speed curve is limited at low flow rate values in order to avoid instability phenomena and these points form the surge line. On the other hand, the maximum flow rate values at each constant speed line are limited by the choking of the flow exiting the compressor's diffuser and these points form the choke line. The operating points corresponding to stable compressor performance lie in between these two lines. Compressor efficiency contours are also superimposed.

The manufacturer's compressor performance maps are most likely given in terms of corrected quantities. The compressor performance maps usually provide curves of pressure ratio versus corrected mass or volumetric flow rate for constant values of corrected shaft speed [4]. The compressor corrected speed and corrected volumetric flow rate are given by the following equations:

$$N_{cor} = N \cdot \sqrt{\frac{T_{ref}}{T_{o1}}} \tag{5.1.1}$$

$$\dot{V}_{cor} = \dot{V} \cdot \sqrt{\frac{T_{o1}}{T_{ref}}} \tag{5.1.2}$$

If the corrected mass flow rate is used, then the following equation is used:

$$\dot{m}_{cor} = \dot{m} \cdot \sqrt{\frac{T_{o1}}{T_{ref}}} \cdot \frac{p_{ref}}{p_{o1}} \tag{5.1.3}$$

The volumetric flow rate and the compressor isentropic efficiency can be calculated at any instant if the instantaneous values of the compressor pressure ratio and the shaft speed, along with the compressor map, are known.

The work required to drive the compressor can be calculated by applying the energy conservation law to a control volume around the compressor. The work transfer rate to the compressor is calculated by the following equation:

$$\dot{W}_C = \dot{m}_C \cdot \left(h_{o2} - h_{o1}\right) + \dot{Q}_C \tag{5.1.4}$$

The total enthalpy of the air at the compressor's outlet can be calculated using the total temperature of the air at the same position, which is calculated using the compressor isentropic efficiency. The total to total isentropic efficiency is defined by the following equation, in reference to Figure 5.1:

$$\eta_{t-t,\mathrm{C}} = \frac{h_{o2,s} - h_{o1}}{h_{o2} - h_{o1}} \tag{5.1.5}$$

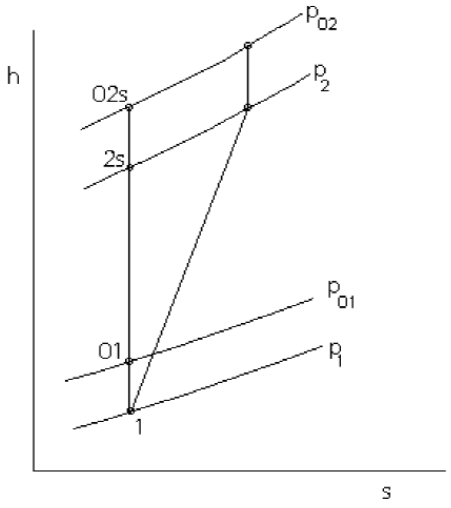

Figure 5.1: *Compressor enthalpy versus entropy thermodynamic diagram [5]*

For an isentropic compression, it is valid to use the following equation:

$$\frac{p_{o2}}{p_{o1}} = \left(\frac{T_{o2,s}}{T_{o1}} \right)^{\frac{\gamma-1}{\gamma}} \tag{5.1.6}$$

Substituting equation (5.1.6) into equation (5.1.5) and assuming constant value for the specific heat capacity at constant pressure throughout the compression process, the total to total isentropic efficiency can be rewritten:

$$\eta_{t-t,\mathrm{C}} = \frac{\left(\frac{p_{o2}}{p_{o1}} \right)^{\frac{\gamma-1}{\gamma}} - 1}{\frac{T_{o2}}{T_{o1}} - 1} \tag{5.1.7}$$

Finally, the total temperature of the air at the compressor's outlet can be calculated using equation (5.1.7), which is written:

$$T_{o2} = T_{o1} \cdot \left[1 + \left(\left(p_{o2} / p_{o1} \right)^{\frac{\gamma-1}{\gamma}} - 1 \right) \Big/ \eta_{t-t,c} \right] \tag{5.1.8}$$

5.1.1 Auxiliary Blower Model

The auxiliary blower is modeled using the static pressure increase versus volumetric flow rate curve at the operational speed of the blower and the standard air density, which is provided by the manufacturer. The standard air density is $1.225\ \mathrm{kg/m^3}$. The static pressure increase of the air passing through the blower is expressed as a quadratic equation of the blower volumetric flow rate and is written:

$$\Delta p_{static,st} = C_1 + C_2 \cdot \dot{V} + C_2 \cdot \dot{V}^2 \tag{5.1.9}$$

A blower connected to a duct and running at constant speed essentially works as a constant volume pump which delivers the same volume of air regardless of the discharge pressure. Though, the density of the air passing through the blower depends on its pressure and temperature. Thus, the static pressure increase that will be finally achieved by the blower operation, depending on the calculated density of the air passing through the blower, can be written:

$$\frac{\Delta p_{static}}{\Delta p_{static,st}} = \frac{\rho}{\rho_{st}} \Rightarrow \Delta p_{static} = \Delta p_{static,st} \cdot \frac{\rho}{\rho_{st}} \tag{5.1.10}$$

While this model for the blower operation is valid for low load engine operation, the compressor – blower interaction during the starting phase of the engine is a lot more complicated. At first, the compressor is completely still, while the blower will start operating. When starting air is admitted into the cylinders, the compressor is rotating at very low speeds, until fuel is injected in the cylinders. Then, increased exhaust temperature and pressure can power the turbine to accelerate the turboshaft. The blower volumetric flow is the one calculated from the previously described compressor model and is invalid during this operating condition. Though, the engine simulation code structure made it quite difficult to change the compressor – blower interaction model.

5.2 Compressor Map Extension

The compressor map provided by the manufacturer typically covers the rotational speed area from 40% to 100% of the maximum turbocharger speed. Thus, the compressor map extension to the lower speed region is required in order to more accurately predict the compressor performance for low load operation.

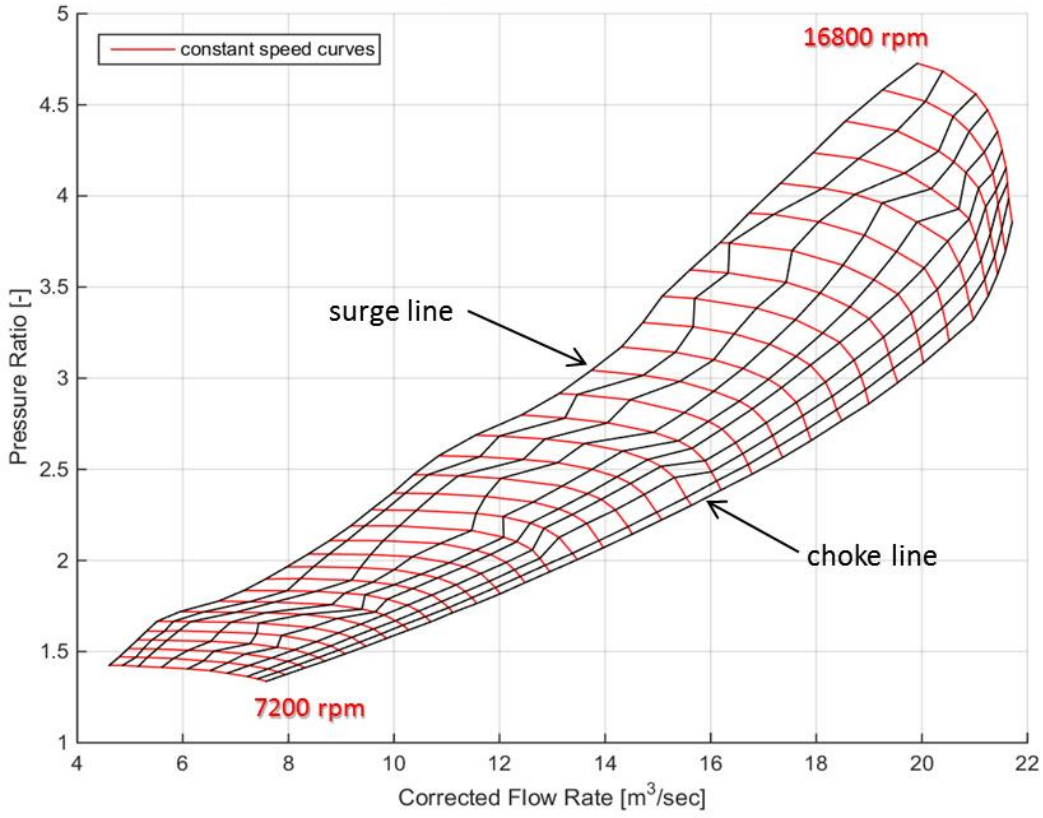

Figure 5.2: *Compressor Map Example*

The compressor map prediction will be based on the non-dimensional parameters used to describe the performance of a compressor. These parameters are the flow coefficient and the isentropic head coefficient, which can be calculated using the following equations:

$$\Phi = \frac{\dot{V}}{A_{imp} \cdot u_{tip}} \tag{5.2.1}$$

$$\Psi = \frac{\pi_c^{\frac{\gamma-1}{\gamma}} - 1}{(\gamma - 1) \cdot M_2^{\,2}} \tag{5.2.2}$$

The Mach number used in equation (5.2.2) refers to the impeller tip linear velocity and is calculated using the following equation:

$$M_2 = \frac{u_{tip}}{\sqrt{\gamma \cdot R \cdot T_{ref}}} = \frac{\pi \cdot N \cdot D_{tip}}{60 \cdot \sqrt{\gamma \cdot R \cdot T_{ref}}} \tag{5.2.3}$$

The isentropic head coefficient can be expressed as a function of the flow coefficient and the Mach number in the following way [7]:

$$\Psi = \frac{k_1 + k_2 \cdot \Phi}{k_3 - \Phi} \tag{5.2.4}$$

where $k_i = k_{i1} + k_{i2} \cdot M_2$ for $i = 1,\ 2,\ 3$.

For a number of given points of compressor constant speed curves, an interpolated surface can be derived using equation (5.2.4). An example of the interpolated surface $\Psi = f(\Phi,\ \mathrm{M}_2)$, using the four lowest compressor constant speed curves is shown in Figure 5.3, where coefficients k_{ij}, $i = 1,\ 2,\ 3\ \&\ j = 1,\ 2$ are calculated using Matlab's Curve Fitting Toolbox.

As far as the compressor isentropic efficiency is concerned, it can be expressed as a second order polynomial of the flow coefficient and a first order polynomial of the Mach number in the following way:

$$\eta_{t-t,\mathrm{C}} = u_1 + u_2 \cdot \Phi + u_3 \cdot \mathrm{M}_2 + u_4 \cdot \Phi^2 + u_5 \cdot \Phi \cdot \mathrm{M}_2 \tag{5.2.5}$$

An example of the interpolated surface $\eta_c = f(\Phi, \mathrm{M}_2)$, using the same given points as before, is shown in Figure 5.4, where coefficients u_i, $i = 1, \ldots, 5$ are calculated using Matlab's Curve Fitting Toolbox.

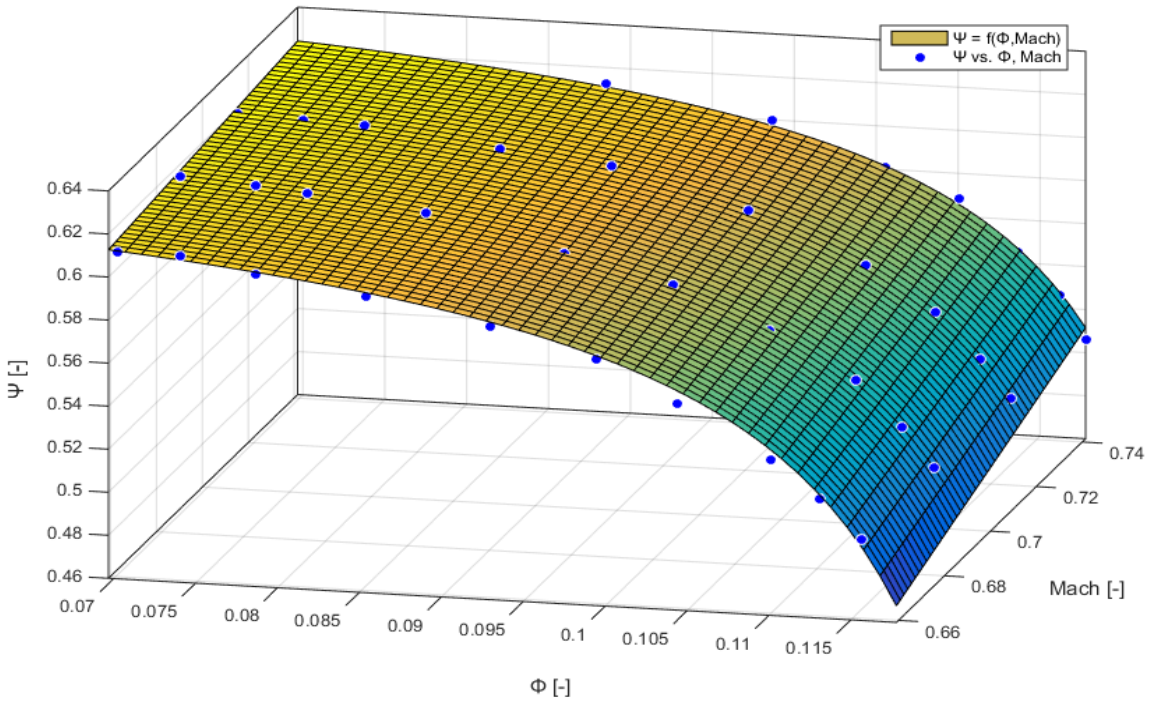

Figure 5.3: *Non –Dimensional Compressor Head Coefficient Interpolated Surface using the four lowest Original Constant Speed Lines*

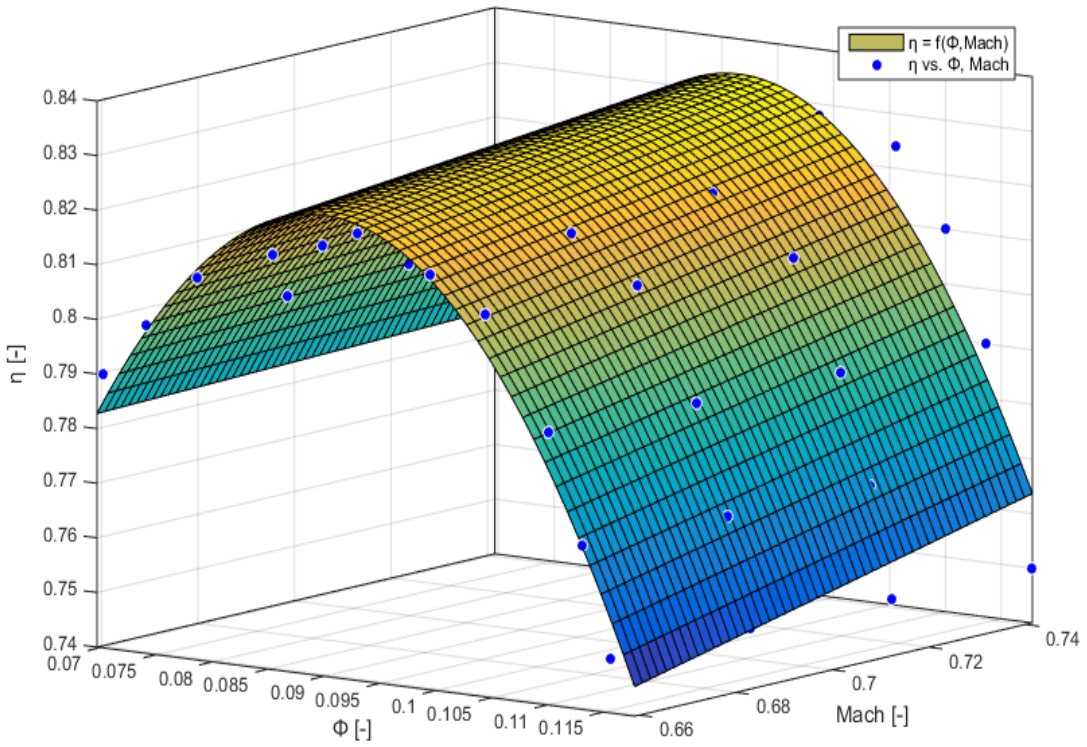

Figure 5.4: *Compressor Isentropic Efficiency Surface Interpolation using the four lowest Original Constant Speed Lines*

Equation (5.2.5) resulted in better interpolated surface, for the given compressor map, than any other found in the bibliography [8], [9], [10].

Using the calculated values of parameters k_{ij}, $i=1, 2, 3$ & $j=1, 2$ and equation (5.2.4), the head coefficient Ψ can be calculated for the desired range of constant Mach numbers corresponding to lower turboshaft speeds and over a range of the flow coefficient Φ. Then, the corrected flow rate $\dot{V}$ and pressure ratio π_C values for the extrapolated constant speed lines can be calculated using equations (5.2.1) and (5.2.2). An example of the constant speed lines resulted from this extrapolation process is shown in Figure 5.5.

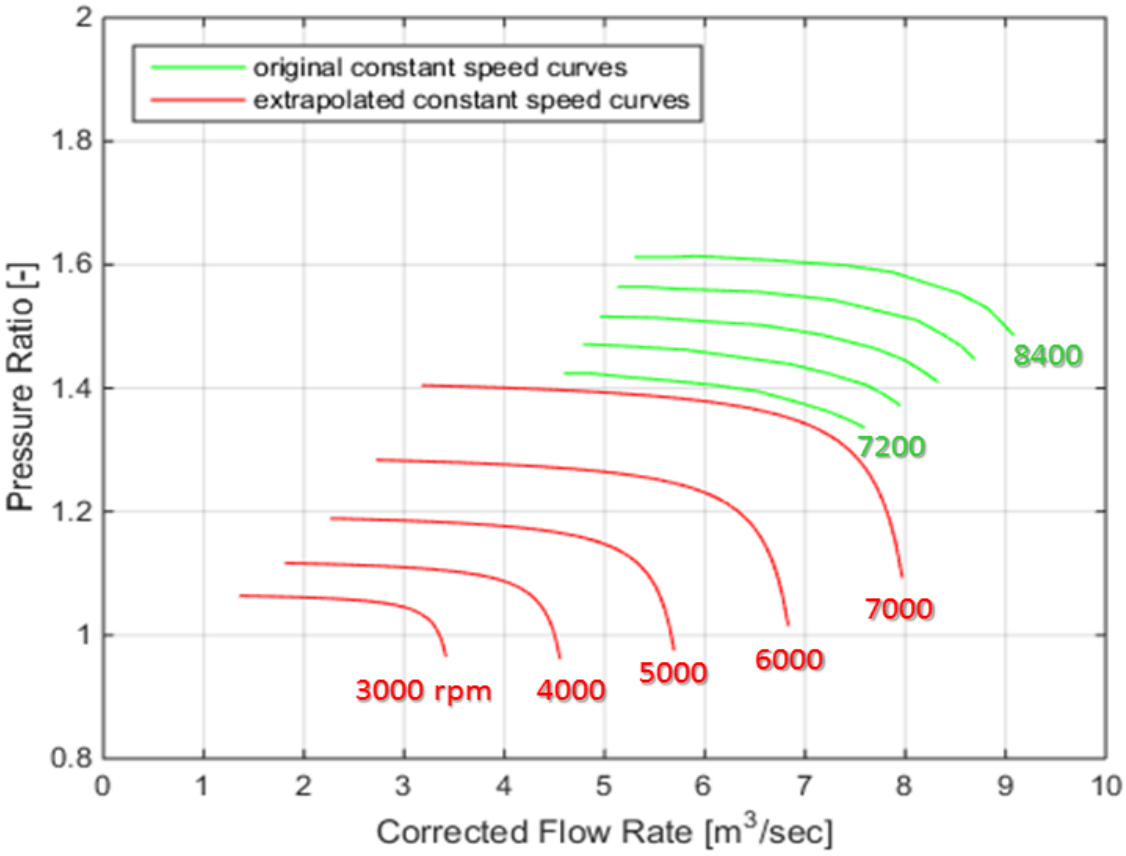

Figure 5.5: *Extrapolated Compressor Constant Speed Lines*

Exactly the same procedure was followed for the extrapolation of the compressor isentropic efficiency. Using the calculated values of the parameters u_i, $i=1, \ldots, 5$ and equation (5.2.5), the isentropic compressor coefficient η_C can be calculated for the desired range of constant Mach numbers corresponding to lower constant turboshaft speeds and over a range of the flow coefficient Φ. The isentropic compressor efficiency can then easily be presented versus the corrected flow rate for constant compressor speed, as shown in Figure 5.6.

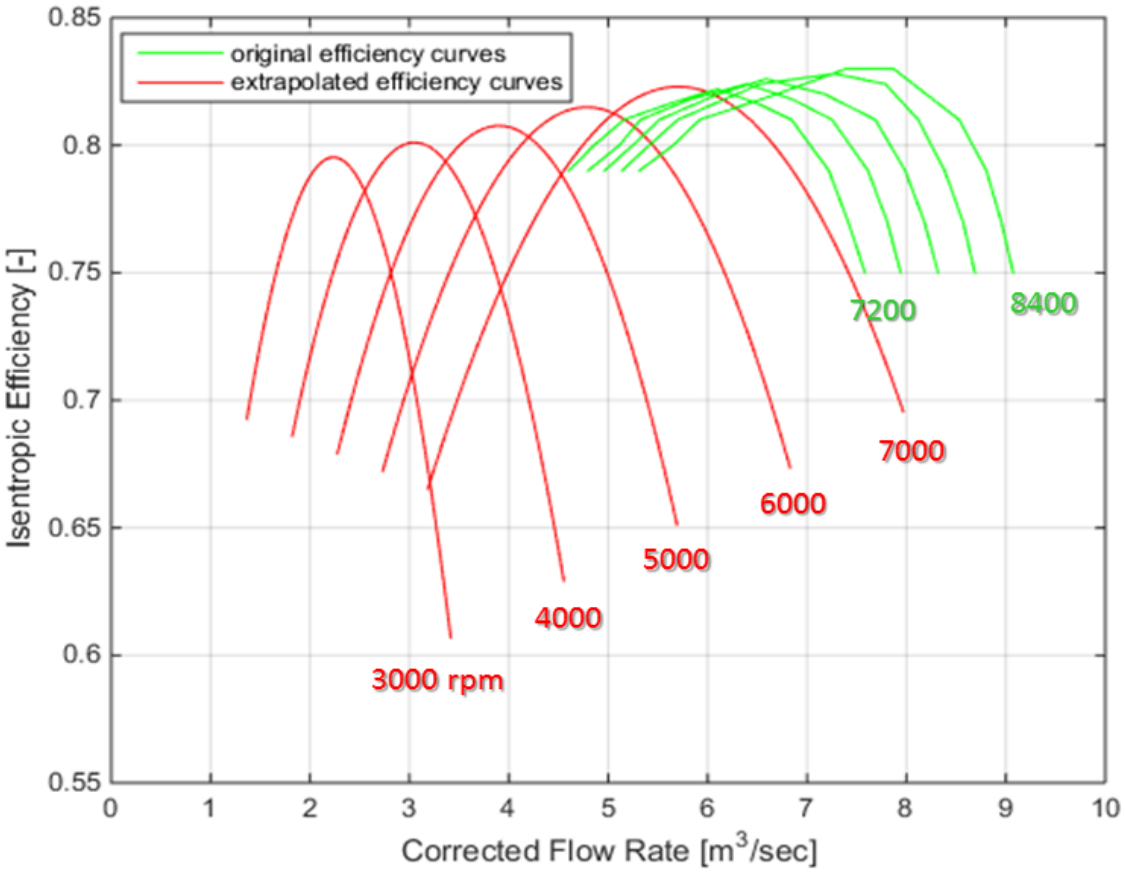

Figure 5.6: *Extrapolated Compressor Isentropic Efficiency for Constant Speed*

5.3 Turbine Modeling

The performance of a turbine is usually modeled using two types of maps, the swallowing capacity map and the efficiency map, both obtained experimentally. The first consists of the turbine mass flow parameter (or swallowing capacity) plotted against the turbine pressure ratio, while the second consists of the turbine isentropic efficiency (usually total to static) plotted against the turbine mass flow parameter.

The turbine mass flow rate and isentropic efficiency can be calculated at any instant if the instantaneous values of the turbine pressure ratio and the shaft speed, along with the two aforementioned turbine maps, are known.

The work transfer rate delivered from the turbine can be calculated using the following equation:

$$\dot{W}_T = \dot{m}_T \cdot (h_{o3} - h_{o4}) - \dot{Q}_T \qquad (5.3.1)$$

The total enthalpy of the working medium exiting the turbine can be calculated using the turbine isentropic efficiency, the equation of isentropic expansion and the relation between static and total temperature. The total to static isentropic efficiency is defined by the following equation, in reference to Figure 5.7:

$$\eta_{t-s,\mathrm{T}} = \frac{T_{o3} - T_{o4}}{T_{o3} - T_{4,s}} \tag{5.3.2}$$

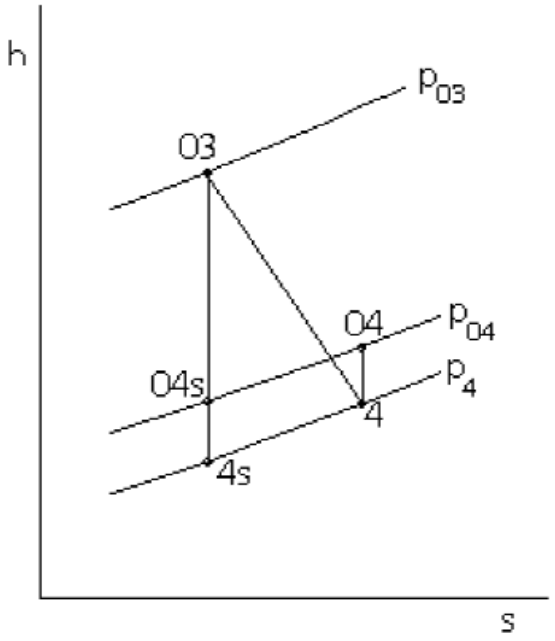

Figure 5.7: *Turbine enthalpy versus entropy thermodynamic diagram [5]*

For an isentropic expansion, it is valid to use the following equation:

$$\frac{p_{o3}}{p_{o4}} = \left(\frac{T_{o3}}{T_{4,s}} \right)^{\frac{\gamma-1}{\gamma}} \tag{5.3.3}$$

Substituting equation (5.3.3) into equation (5.3.2) and assuming constant value for the specific heat capacity at constant pressure throughout the expansion process, the turbine total to static isentropic efficiency can be written:

$$\eta_{t-s,\mathrm{T}} = \frac{1 - \left(\frac{T_{o4}}{T_{o3}} \right)}{1 - \left(\frac{p_4}{p_{o3}} \right)^{\frac{\gamma-1}{\gamma}}} \tag{5.3.4}$$

The total temperature of the gas at the turbine's outlet can be derived from equation (5.3.4), which can be written:

$$T_{o4} = T_{o3} \cdot \left\{ 1 - \eta_{t-t,c} \cdot \left[1 - \left(p_4 / p_{o3} \right)^{\frac{\gamma-1}{\gamma}} \right] \right\} \tag{5.3.5}$$

Then, the static temperature of the gas exiting the turbine can be calculated using the following equation:

$$T_4 = T_{o4} - \frac{u_{dif}^{\ 2}}{2 \cdot c_p} \tag{5.3.6}$$

The velocity of the working medium is obtained using the mass flow equation as follows:

$$\dot{m}_T = \rho \cdot A_{dif} \cdot u_{dif} \Rightarrow u_{dif} = \frac{\dot{m}_T}{\rho \cdot A_{dif}} \tag{5.3.7}$$

Finally, the static pressure of the gas exiting the turbine can be calculated using the isentropic expansion equation for static to total ratios of pressure and temperature at the same position (see Figure 5.7):

$$p_4 = p_{o4} \cdot \left(\frac{T_4}{T_{o4}} \right)^{\frac{\gamma}{\gamma-1}} \tag{5.3.8}$$

5.4 Turbine Map Extension

As was the case with compressor maps, turbine maps typically cover the rotational speed area from 40% to 100% of the maximum turbocharger speed. Thus, the extension of the turbine map is required in order to predict the low load operation of the turbine.

The original points of the swallowing capacity map are interpolated using a cubic spline interpolation method, including the axis intersection point. The interpolation method was executed using Matlab's Curve Fitting Toolbox. Using the calculated values of the spline coefficients, a sufficient number of points corresponding to low load operation was calculated. The swallowing capacity map used to predict the performance of the turbine for low load operation, is presented in Figure 5.8.

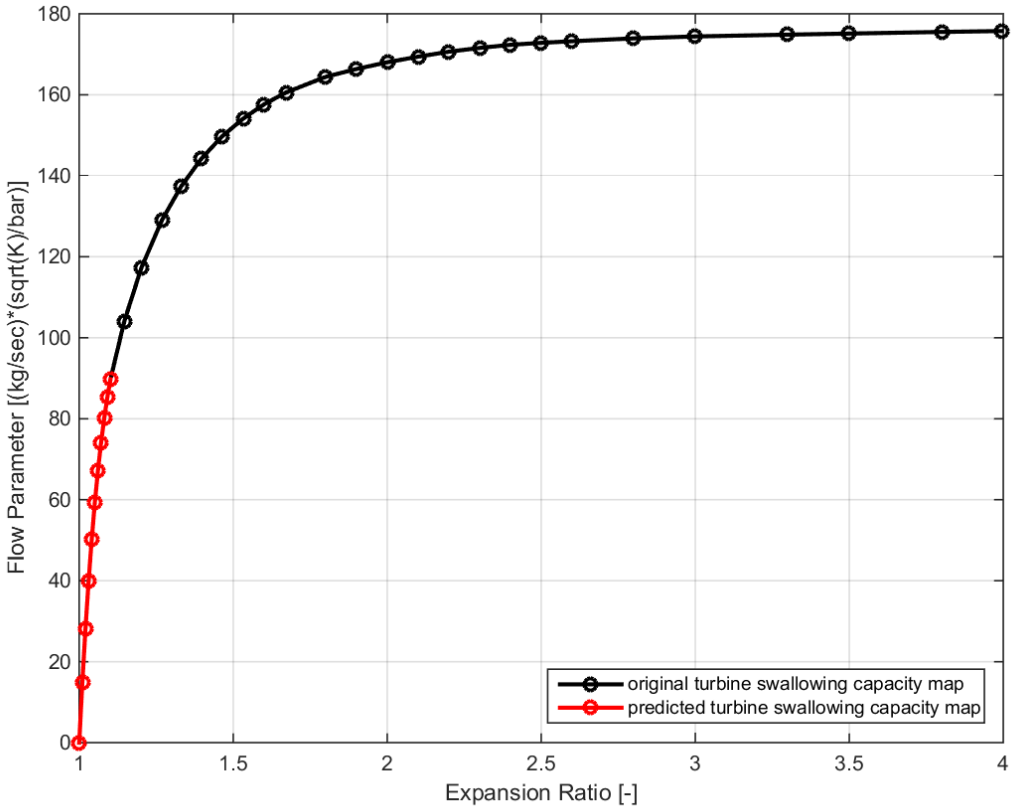

Figure 5.8: *Turbine's Swallowing Capacity Map*

6 Engine – Propeller - Ship Interaction

The most common agent employed to produce thrust and move a ship is a single screw propeller. The primary source of propeller power is a two-stroke diesel engine. In most cases the engine is directly connected to the propeller without the use of a clutch or a gear unit. Thus, it is necessary to calculate the propeller toque demand transient operating conditions. The prediction of the propeller load requires the calculation of the advance speed, hence, a ship surge model is also used.

Generally, there are two main types of marine propellers, the fixed pitch propeller (FPP) and the controllable pitch propeller (CPP). Ordinary merchant ships, like containerships, bulk carriers and crude oil tankers, which do not require a high degree of manoeuvrability, are equipped with fixed pitch propellers. Furthermore, FPPs are less expensive and involve lower risk of problems during service than controllable pitch propellers [11]. In the present thesis a model for fixed pitch propellers is used.

6.1 Four-Quadrant Propeller Modeling

The most conventional way of operating a propeller is with positive rotational speed and inflow velocity. Nonetheless, the propeller sometimes has to produce thrust in the reverse direction, propelling the ship astern. Also, it can be used to decelerate the ship by running in the opposite direction of the advance speed [12].

In the present thesis, a four quadrant propeller performance model will be used in order to enable the simulation of any operating condition of the propulsion system. In the case of a fixed pitch propeller the operation in four quadrants is defined based on the advance angle at the 70% of the propeller radius:

$$\beta = \arctan\left(\frac{V_a}{0.7 \cdot \pi \cdot n \cdot D_p}\right) \tag{6.1.1}$$

The basic advantage of the four quadrant propeller performance model lies in the use of the advance angle, in comparison to the conventional propeller performance models, where propeller characteristics are defined based on the advance coefficient $J = V_a / \left(n \cdot D_p\right)$. That' s because, in simulations requiring propeller performance prediction in more than one quadrant, advance coefficient J can take an infinite value when propeller speed is equal to zero. If the shaft speed is

equal to zero, the advance angle is equal to 90° or 270°, depending on the direction of the advance speed.

Quadrant	Advance Speed	Rotational Speed	Advance Angle
1st	ahead	ahead	$0 \le \beta \le 90^{o}$
2nd	ahead	astern	$90^{o} \le \beta \le 180^{o}$
3rd	astern	astern	$180^{o} \le \beta \le 270^{o}$
4th	astern	ahead	$270^{o} \le \beta \le 360^{o}$

Table 6.1: *Propeller four quadrants of operation*

The four quadrants represent the four potential combinations of propeller shaft rotational speed and advance speed, as shown in Table 6.1 and Figure 6.1. The first quadrant corresponds to the most common combination where both the propeller speed and the advance speed have positive values, while the second quadrant represents the operating condition of a decelerating ship, where the propeller speed is negative and the advance speed is positive. Furthermore, the third quadrant corresponds to the operating condition of a ship moving in the astern direction, where both the propeller speed and the advance speed have negative values. Lastly, in the fourth quadrant of operation the ship is moving in the astern direction and the propeller produces positive thrust.

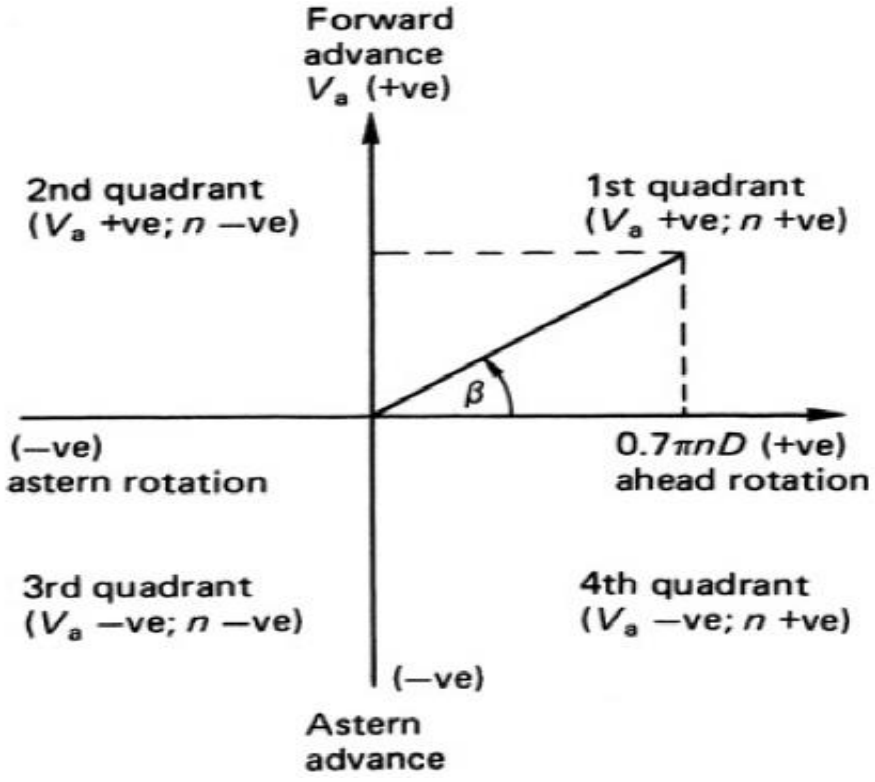

Figure 6.1: *Propeller four quadrants of operation [13]*

The propeller characteristics in four quadrants of operation are usually described using non-dimensional parameters. The thrust and torque coefficients can be based on experimentally obtained periodic functions of the advance angle. The following Figure 6.2 shows an example of such experimentally obtained data for the Wageningen B-Series four bladed propellers.

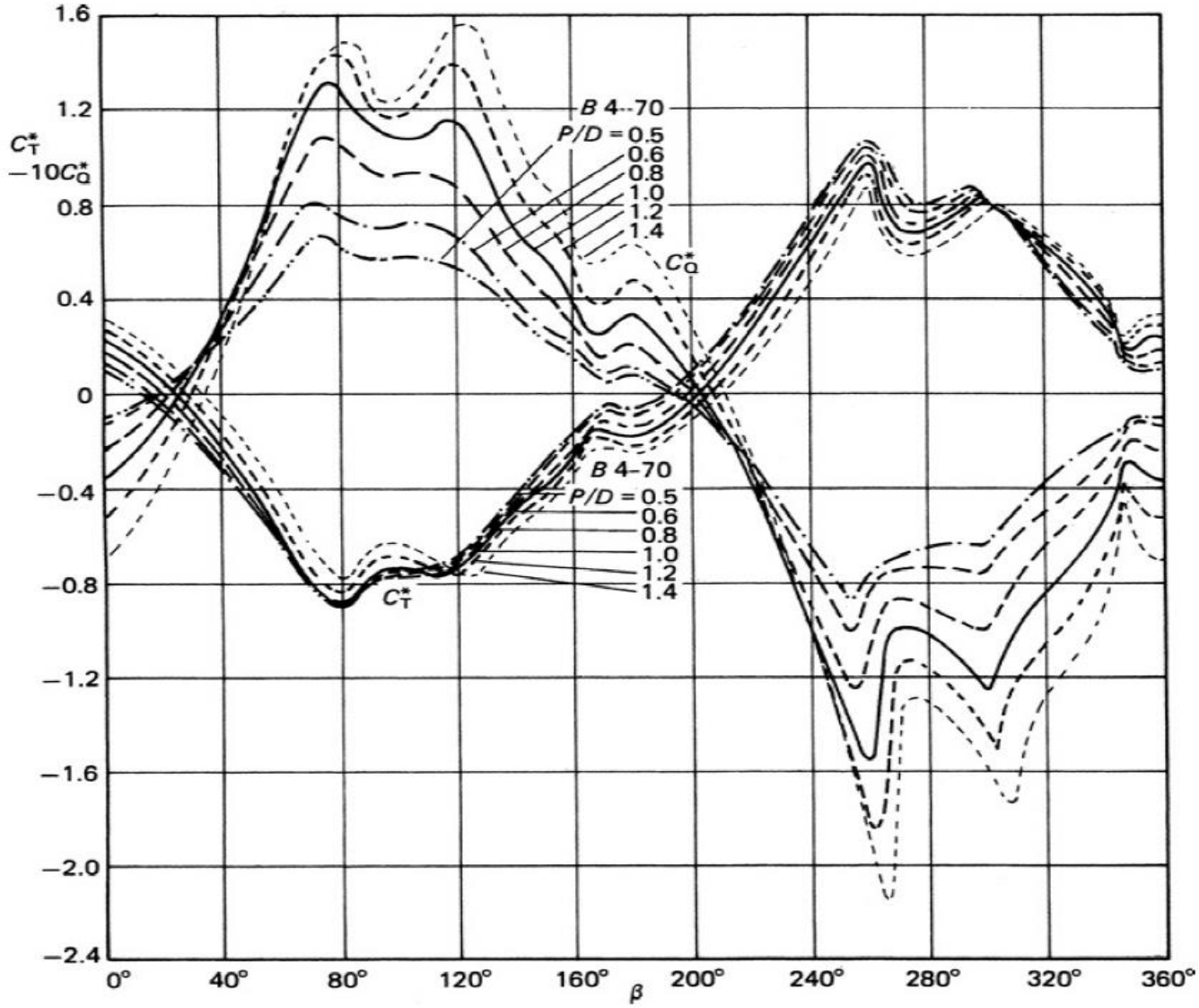

Figure 6.2: *Open Water Test Results for Wageningen B4-70 Screw Series over a range of* P/D *values in four quadrants [13]*

The non-dimensional thrust and torque propeller coefficients are written as a function of the relative advance velocity $V_r^2 = V_a^2 + \left(0.7 \cdot \pi \cdot n \cdot D_p\right)^2$, so the following equations are derived:

$$C_T^* = \frac{T_p}{\frac{1}{2} \cdot \rho_{sw} \cdot V_r^2 \cdot A_0} \tag{6.1.2}$$

$$C_Q^* = \frac{Q_p}{\frac{1}{2}\cdot \rho_{sw} \cdot V_r^2 \cdot A_0 \cdot D_p} \tag{6.1.3}$$

Substituting in equations (6.1.2) and (6.1.3) the relations for the propeller disk area A_0 and the relative advance velocity V_r, the following equations are derived:

$$C_T^* = \frac{T_p}{\frac{\pi}{8}\cdot \rho_{sw} \cdot \left[V_a^2 + \left(0.7\cdot \pi \cdot n \cdot D_p^2\right)\right] \cdot D_p^2} \tag{6.1.4}$$

$$C_Q^* = \frac{Q_p}{\frac{\pi}{8}\cdot \rho_{sw} \cdot \left[V_a^2 + \left(0.7\cdot \pi \cdot n \cdot D_p^2\right)\right] \cdot D_p^3} \tag{6.1.5}$$

For modeling purposes, the propeller thrust and torque coefficients can be seen as periodic functions over the range over the range $0 \le \beta \le 360^o$ and can be calculated using a Fourier type representation, which can be written as follows:

$$C_T^* = \sum_{k=1}^{m} \left[A_k \cdot \cos\left(k\cdot\beta\right) + B_k \cdot \sin\left(k\cdot\beta\right)\right] \tag{6.1.6}$$

$$C_Q^* = \sum_{k=1}^{m} \left[A_k \cdot \cos\left(k\cdot\beta\right) + B_k \cdot \sin\left(k\cdot\beta\right)\right] \tag{6.1.7}$$

6.2 Propeller Shaft Dynamics

Fixed Pitch Propellers are directly connected to the engine crankshaft, which is modeled using a mechanical element. The angular acceleration of a mechanical element is calculated using equation (3.2.18). For the crankshaft being directly connected with the propeller, equation (3.2.18) can be rewritten:

$$\frac{dn}{dt} = \frac{30\cdot\left[\sum_{i=1}^{N_{cyl}}\left(\tau_i\right) - Q_p - Q_{fr}\right]}{I_{eng} + I_p + I_{added-p}} \tag{6.2.1}$$

The propeller contributes to the shafting system total polar moment of inertia with two terms, the propeller's dry polar moment of inertia I_p and the propeller's entrained water inertia or added polar moment of inertia $I_{added-p}$.

6.2.1 Dry propeller inertia

By definition, the polar mass moment of inertia of a rotating body is the sum of all element masses multiplied by the square of their distance from a reference axis. However, this is not a particularly helpful approach for the calculation of the dry propeller inertia. So, the propeller's blade moment of inertia is calculated using a Simpson's numerical integration method using an odd number of propeller blade sections. The calculations required are shown in the following Table 6.2.

x=r/R	A_x	Simpson Multipliers	$A_x \cdot SM$	1st moment arm	$A_x \cdot SM \cdot$ 1st MA	2st moment arm	$A_x \cdot SM \cdot$ 1st MA $\cdot$ 2nd MA
[1]	[2]	[3]	[4] =[2]·[3]	[5]	[6] =[5]·[4]	[7]	[8] =[7]·[6]
1.0	A_{x1}	0.5	$0.5 \cdot A_{x1}$	0	0	0	0
x_2	A_{x2}	2	$2 \cdot A_{x2}$	1	$2 \cdot A_{x2}$	1	$2 \cdot A_{x2}$
x_3	A_{x3}	1	A_{x3}	2	$2 \cdot A_{x3}$	2	$4 \cdot A_{x3}$
x_4	A_{x4}	2	$2 \cdot A_{x4}$	3	$6 \cdot A_{x4}$	3	$18 \cdot A_{x4}$
x_5	A_{x5}	1	A_{x5}	4	$4 \cdot A_{x5}$	4	$16 \cdot A_{x5}$
x_6	A_{x6}	2	$2 \cdot A_{x6}$	5	$10 \cdot A_{x6}$	5	$50 \cdot A_{x6}$
x_7	A_{x7}	1	A_{x7}	6	$6 \cdot A_{x7}$	6	$36 \cdot A_{x7}$
x_8	A_{x8}	2	$2 \cdot A_{x8}$	7	$14 \cdot A_{x8}$	7	$98 \cdot A_{x8}$
x_9	A_{x9}	1	A_{x9}	8	$8 \cdot A_{x9}$	8	$64 \cdot A_{x9}$
x_{10}	A_{x10}	2	$2 \cdot A_{x10}$	9	$18 \cdot A_{x10}$	9	$162 \cdot A_{x10}$
x_h	A_{xh}	0.5	$0.5 \cdot A_{xh}$	10	$5 \cdot A_{xh}$	10	$50 \cdot A_{xh}$
			Σ_1		Σ_2		Σ_3

Table 6.2: *Propeller Blade Moment of Inertia Calculation Method [13]*

Using the results from Table 6.2, the volume moment of inertia of a propeller blade can be estimated about the propeller tip from the following equation [13]:

$$I_{tip} = \frac{2}{3} \cdot \left(\frac{\left(\frac{D_p}{2} \right) - r_h}{10} \right)^3 \cdot \Sigma_3 \qquad (6.2.2)$$

The moment of inertia of the blade can be estimated in reference to the center of the propeller shaft by applying the parallel axis theorem twice, according to the following equation [13]:

$$I_{blade} = \rho_p \cdot \left[I_{tip} + \frac{2}{3} \cdot \Sigma_1 \cdot \left(\left(\frac{D_p}{2} \right) - r_h \right) \cdot \left({r_{ct-tip}}^2 - {r_{ct-shaft}}^2 \right) \right] \qquad (6.2.3)$$

The radial distance of the blade's centroid from the tip r_{ct-tip} and from the shaft $r_{ct-shaft}$ can be calculated using the following equations [13]:

$$r_{ct-tip} = \frac{\left(D_p/2\right) - r_h}{10} \cdot \frac{\Sigma_2}{\Sigma_1} \tag{6.2.4}$$

$$r_{ct-shaft} = \left(D_p/2\right) - r_{ct-tip} \tag{6.2.5}$$

Finally, if the polar moment of inertia of the propeller's hub I_h, is calculated, the propeller's total polar mass moment of inertia can be written:

$$I_p = I_h + Z \cdot I_{blade} \tag{6.2.6}$$

6.2.2 Added propeller inertia

When propellers are immersed and rotating in water, their inertia characteristics are changed due to their interaction with the water carried along. This leads to an augmentation of their mass properties values. While the dry propeller inertia can be calculated with an adequate precision using volumetric calculations, entrained water inertia can vary significantly. It is usually found in the range of 5-30% of the dry propeller inertia. In the present thesis, the added propeller inertia was considered to be the mean value of the added propeller inertia derived from the application of two different estimation methods [13], [14].

Both methods are basically proposing a different way of calculating the non-dimensional added propeller inertia $C_k = I_{p-added} \Big/ \left(\rho_{sw} \cdot D_p{}^5\right)$. Then, the added propeller inertia can be calculated using the following equation:

$$I_{added-p} = C_k \cdot \rho_{sw} \cdot D_p{}^5 \tag{6.2.7}$$

Parsons Estimates

The first method was proposed by Parsons and is based on the statistical analysis of numerical calculations for Wageningen B-Series propellers, using specialized lifting-line and lifting-surface theory methods [14]. The non-dimensional entrained water inertia is calculated using the following equation:

$$C_{Parsons} = C \cdot LSC \tag{6.2.8}$$

The C-factor and LSC-factor in the above equation are given as a function of propeller's geometric parameters, such as the expanded area ratio (EAR), the pitch to diameter ratio $\left(P/D\right)$, a parameter describing the blade's aspect ratio (AR) and six coefficients depending on propeller blade number Z. The blade's aspect ratio is considered to be $AR = 0.22087 \cdot \left(Z/EAR\right)$. For four bladed propellers the two factors are calculated using the following equations:

$$\begin{aligned} C = {} & 0.00303 - 0.00808 \cdot EAR - 0.00407 \cdot \left(\frac{P}{D}\right) \\ & + 0.00341 \cdot EAR^2 + 0.00043 \cdot \left(\frac{P}{D}\right)^2 + 0.00997 \cdot EAR \cdot \left(\frac{P}{D}\right) \end{aligned} \tag{6.2.9}$$

and

$$\begin{aligned} LSC = {} & 0.61046 + 0.34674 \cdot \left(\frac{P}{D}\right) + 0.60294 \cdot AR^{-1} \\ & -0.56159 \cdot AR^{-2} - 0.80696 \cdot \left(\frac{P}{D}\right) \cdot AR^{-1} + 0.45806 \cdot \left(\frac{P}{D}\right) \cdot AR^{-2} \end{aligned} \tag{6.2.10}$$

Schwanecke Estimates

The second method was proposed by Schwanecke. He suggested an estimation of the added propeller inertia for propellers of ordinary merchant ships. The non-dimensional value is calculated using the following equation:

$$C_{Schwanecke} = \frac{0.0703 \cdot \left(P/D\right)^2 \cdot EAR^2}{\pi \cdot Z} \tag{6.2.11}$$

6.3 Ship Surge Model

In order to calculate the propeller performance characteristics, the advance speed V_a has to be calculated. The advance speed is the ship's speed V_s reduced according to the wake fraction coefficient w because the propeller is operating at the ship's hull disturbed wake flow and can be written:

$$V_a = (1 - w) \cdot V_s \tag{6.3.1}$$

The ship's speed can be calculated at any instant by applying the linear momentum equation:

$$\left(M_s + M_{added}\right)\cdot \dot{V}_s = (1-t)\cdot T_p - R_T \tag{6.3.2}$$

The ship's mass M_s , which is equal to its displacement, is increased by the ship's added mass M_{added} . The calculation of the ship's added mass is a complicated problem of hydrodynamics and it will be considered equal to a fraction of ship's mass.

In the right hand side of the momentum equation (6.3.2), the thrust produced by the propeller is reduced according to the thrust deduction coefficient t . The operation of the propeller in the back end of the hull and their interaction results in the augmentation of ship's hull resistance. This means that the thrust force produced by the propeller has to overcome both the ship's bare hull total resistance R_T and the aforementioned extra resistance.

Both the wake fraction and the thrust deduction coefficients depend on the shape of the hull. For ships with one propeller the wake fraction coefficient is normally in the region of 0.20 to 0.45, while the thrust deduction coefficient is in the region of 0.12 to 0.30 [11].

The ship's total resistance, which comprises of frictional, residual and air resistance can be written as a function of the total resistance coefficient C_T , which normally depends on the shape of the hull, the ship's speed V_s , the wetted surface area S and the sea water density ρ_{sw} :

$$R_T = \frac{1}{2}\cdot C_T \cdot \rho_{sw} \cdot S \cdot V_s^2 \tag{6.3.3}$$

Due to lack of detailed data concerning the ship's hull shape, an equivalent total resistance coefficient will be introduced. This equivalent total resistance coefficient can be written:

$$C_{T-eq} = \frac{1}{2}\cdot C_T \cdot \rho_{sw} \cdot S \tag{6.3.4}$$

Then, the ship's total resistance can be rewritten using the equivalent total resistance coefficient in the following way:

$$R_T = C_{T-eq} \cdot V_s^2 \tag{6.3.5}$$

If a ship is travelling at a given constant speed, the ship's acceleration is equal to zero and equation (6.3.2) becomes:

$$(1-t)\cdot T_p = R_T \tag{6.3.6}$$

Substituting equation (6.1.2) into in equation (6.3.6) and rearranging for the equivalent total resistance coefficient, the following equation is derived:

$$C_{T-eq} = \frac{(1-t)\cdot\frac{1}{2}\cdot C_T^{\,*}\cdot\rho\cdot V_r^{\,2}\cdot A_0}{V_s^{\,2}} \tag{6.3.7}$$

If the ship's speed and the engine speed are known for a steady state condition, then the equivalent total resistance coefficient can be calculated using equation (6.3.7). For any other speed of the ship, the corresponding total resistance can be calculated using equation (6.3.5).

7 Simulation Setup and Results

The derived models were used for the performance prediction of a representative large marine two-stroke diesel engine during its initial starting and acceleration. The selected engine is the six cylinder MAN B&W S70MC. It's a two-stroke, slow speed, large bore, uniflow scavenged engine and it is considered to be of the reversible type, i.e. directly coupled to a Fixed Pitch Propeller. The engine had already been configured in the MOTHER engine simulation code and used in previous studies for its performance prediction under steady state loading conditions. Steady state runs at 110%, 100%, 75%, 50% and 25% load were performed. For the simulation at 25% load, the electrically driven auxiliary blowers were considered to be activated. Thus, most of the parameters concerning engine's sub-models, such as heat transfer and combustion models, have been calibrated. Nevertheless, the addition of some elements was necessary in order to simulate the engine performance during its starting phase.

7.1 Engine Characteristics

The selected MAN B&W 6S70MC engine is used as the main engine of a Suezmax Tanker. The basic engine characteristics are presented in the following Table 7.1, while the engine cross section is shown in Figure 7.1.

MAN B&W 6S70MC		
No. of Cylinders	6	
Bore	700 mm	
Stroke	2,800 mm	
Compression Ratio	17.57	
Power/cylinder	3,110 kW	
Engine Speed	91 rpm	
Mean effective pressure	19 bar	
Firing Order	1-5-3-4-2-6	
Turbocharger unit(s)	2 x ABB TPL 77	
Auxiliary Blowers	2 x 71 kWe	
Starting Air Reservoir(s) Volume	Reversible Engine	2 x 8.0 m^3
	Non-Reversible engine	2 x 4.5 m^3
Starting Air Compressor Capacity	Reversible Engine	480 m^3/h
	Non-Reversible engine	270 m^3/h

Table 7.1: *MAN B&W 6S70MC-C parameters*

Each engine cylinder has a corresponding phase angle value, which is determined by the crankshaft construction. Cylinder No.1 is considered to be the reference cylinder and its phase angle is set to zero degrees. The phase angle of the other cylinders is derived in accordance with the position of the reference cylinder position and the firing order.

Cylinder No.	1	2	3	4	5	6
Phase angle	0^o	120^o	240^o	180^o	300^o	60^o

Table 7.2: *Phase Angle of each Cylinder*

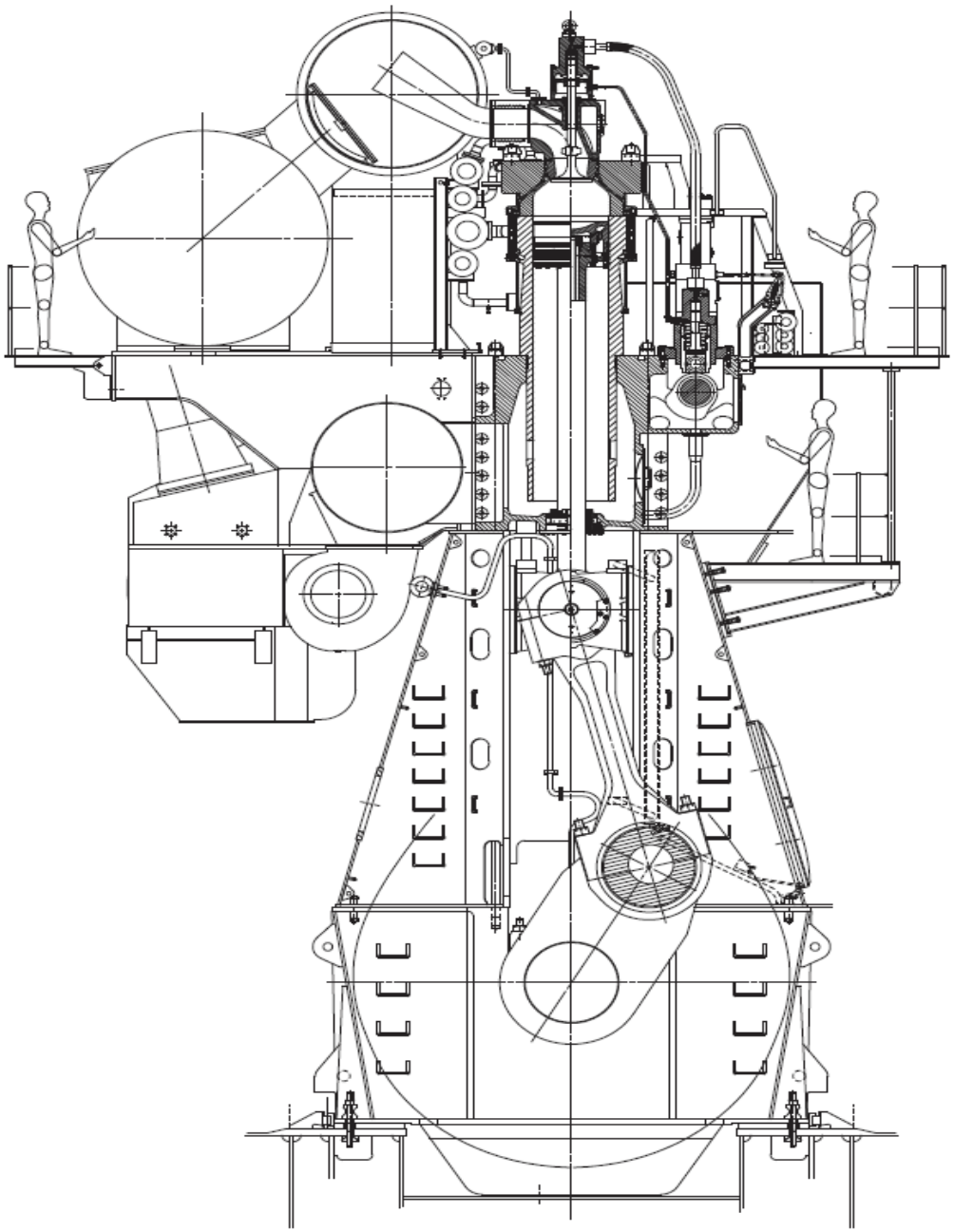

Figure 7.1: *MAN B&W S70MC-C7 Engine Cross Section [1]*

The engine is equipped with two ABB TPL 77 turbochargers. The choice of the turbocharger is usually made in order to obtain the lowest possible values of Specific Fuel Oil Consumption (SFOC) at the nominal MCR. Engines are normally equipped with as few turbochargers as possible, but more turbochargers can be fitted if this is desirable due to space requirements or other reasons. The basic characteristics of the ABB TPL 77 turbocharger are presented in Figure 7.2 and Table 7.3.

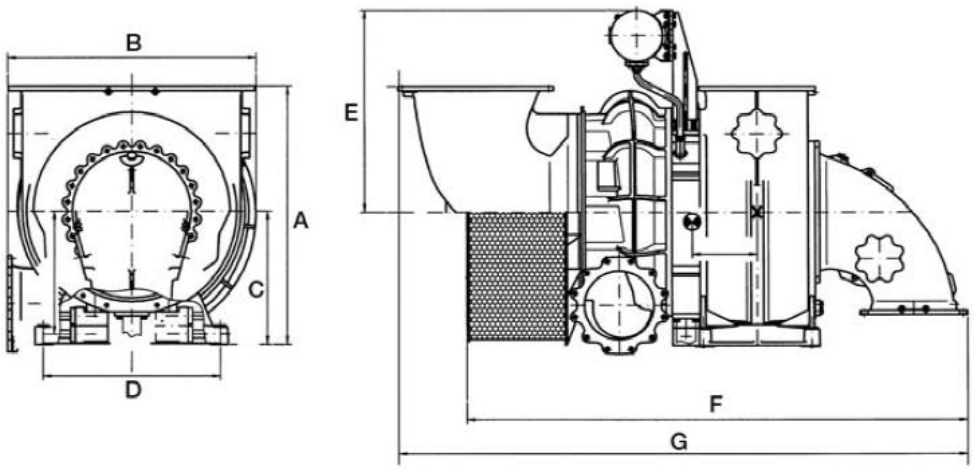

Figure 7.2: *Turbocharger Unit Casing Diagram [ABB Brochure]*

Type	A	B	C	D	E	F	G	Weight
TPL 77-B	1416	1371	732	978	1075	2716	3090	3680

Table 7.3: *Turbocharger Unit Casing Geometry and Weight [ABB Brochure]*

7.2 Propeller Characteristics

The propulsion engine being simulated is considered to be directly connected to a Fixed Pitch Propeller. Due to lack of specific data concerning the real propeller of the propulsion plant and the limited number of propellers provided with experimental data on four-quadrants of operation, the propeller choice became quite restricted. A Wageningen B-series, four-bladed propeller was chosen and its basic characteristic are presented in Table 7.4

The diameter of the propeller was derived from the usual propeller diameter corresponding to ships of the same type and size. The expanded area and pitch to diameter ratios were chosen so as the propeller's torque demand at the nominal revolutions and the engine's output torque at the same revolutions, were matched.

Propeller Characteristics	
Type	Wageningen B-Series
No. of Blades	4
Diameter	7.87 m
Expanded Area Ratio	0.70
Pitch-Diameter Ratio	0.80

Table 7.4: *Propeller Characteristics used in the Simulation Setup*

The open-water performance characteristics of the propeller for the four-quadrants of operation, are presented in the following Figure 7.3, The coefficients A_k and B_k used in equations (6.1.6) and (6.1.7) to calculate the thrust and torque coefficients of the propeller are presented in Table 7.5

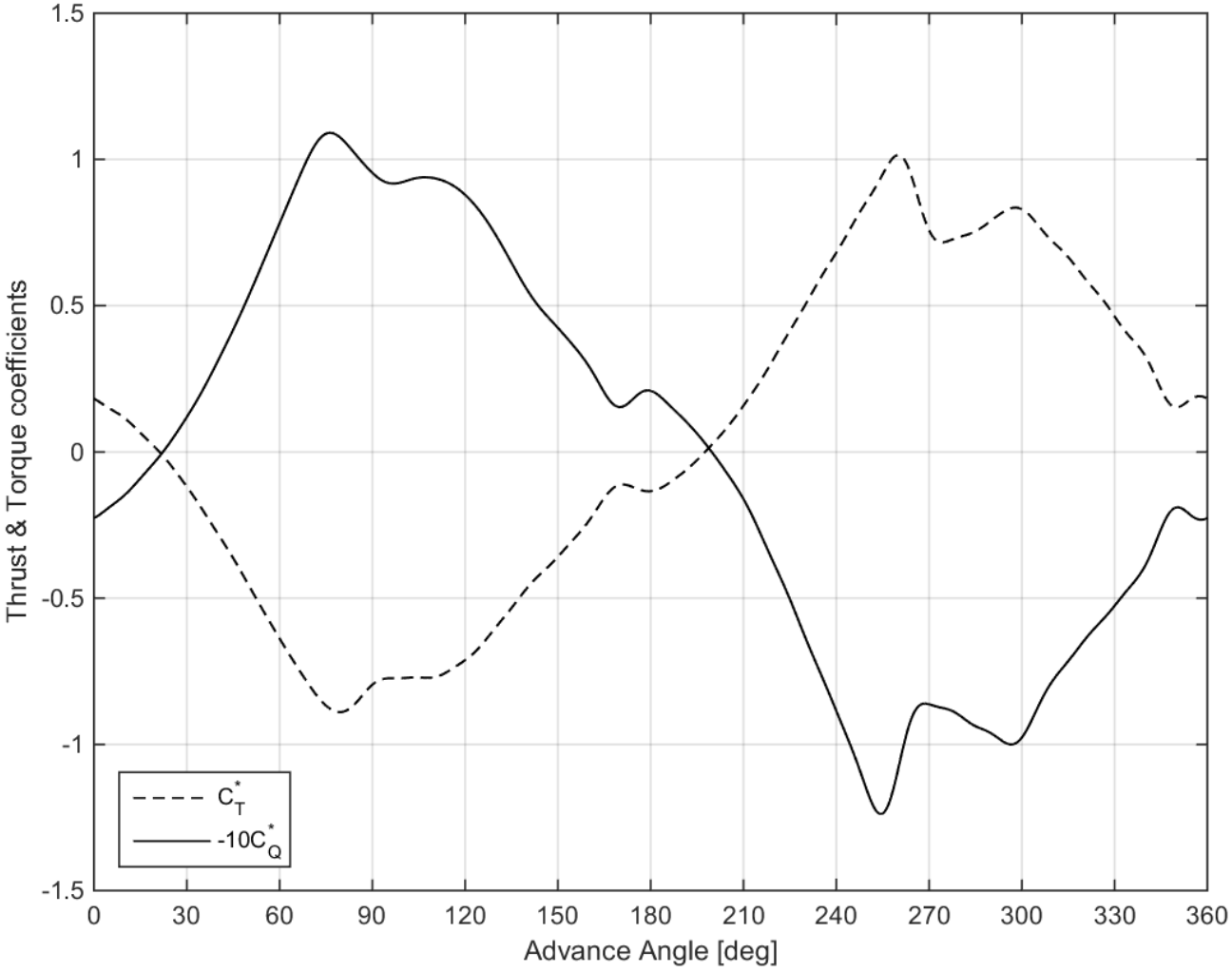

Figure 7.3: *Wageningen B4-70, P/D=0.8 open water characteristics in four quadrants of operation*

	Torque Coefficients		Thrust Coefficients	
k	A_k	B_k	A_k	B_k
0	-2.578300	0.000000	2.875700	0.000000
1	-15.727000	93.080000	13.007000	-77.762000
2	-0.689600	-0.204820	0.628690	-1.303200
3	-5.440200	-13.786000	2.810400	10.580000
4	2.467400	1.558800	-1.683200	-1.041300
5	5.071700	-6.895300	-4.489400	4.576900
6	-1.196400	-0.197730	0.377030	1.429600
7	-3.116100	3.129500	3.164700	-0.396120
8	1.583800	-0.011366	-0.134920	-0.991700
9	1.492500	-4.096700	-1.990500	2.075900
10	-0.908980	-0.328100	0.175760	0.901530
11	-1.213500	0.795390	1.975000	-0.029877
12	0.501260	-0.266240	-0.110630	-0.563540
13	-1.414300	-1.453600	-0.069828	0.947730
14	-0.188730	0.686660	0.256650	0.236810
15	0.154220	0.454990	0.806810	-0.532040
16	0.172940	-0.847920	-0.187810	-0.071537
17	-1.333000	-0.159110	0.298210	0.527680
18	-0.226200	0.597330	0.486430	0.017400
19	0.142990	0.254450	0.338930	-0.681050
20	-0.045335	-0.219910	-0.268510	-0.204000
21	-0.400510	0.475350	0.096098	0.140860
22	0.206290	0.153970	0.214500	-0.057914
23	-0.069705	-0.073692	0.066440	-0.448980
24	-0.182540	-0.022654	-0.132100	-0.114540
25	-0.056307	0.472560	0.016378	-0.012005
26	0.242820	0.130610	0.012367	-0.119320
27	0.079606	-0.061311	-0.161130	-0.244270
28	-0.069503	0.009769	-0.105360	0.049882
29	0.080075	0.131020	-0.041139	0.063587
30	0.042156	-0.019047	-0.008957	-0.073611

Table 7.5: *Harmonic Coefficients for B4-70, P/D=0.8 four-quadrant open water propeller characteristics [15]*

7.3 Simulation Setup

The engine configuration was introduced in the MOTHER engine simulation and performance prediction code. As was described in Chapter 3, the engine is considered to be a series of flow receivers interconnected via flow controllers, complemented by mechanical elements for the transfer of mechanical work. The engine configuration that was used to perform the steady state load runs is showed in Figure 7.4. The thermodynamic and mechanical elements used to configure the engine structure, are presented In Table 7.6.

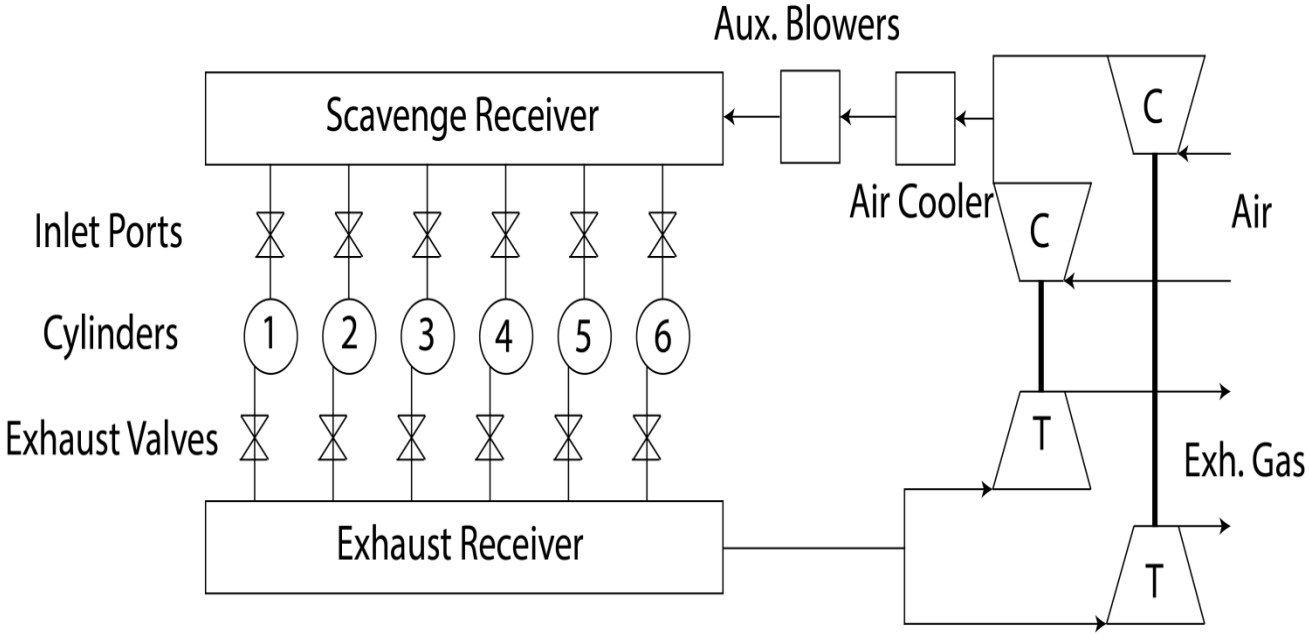

Figure 7.4: *MAN B&W 6S70MC – Engine Configuration*

Thermodynamic elements		**Mechanical elements**
Flow Receivers	**Flow Controllers**	
Scavenge receiver	Inlet ports	Crankshaft
Cylinders	Exhaust Valves	Turboshaft
Exhaust Receiver	Compressor	
Inlet Fixed Fluid	Turbine	
Exhaust Fixed Fluid		

Table 7.6: *Thermodynamic and Mechanical elements of the initial Engine Configuration*

The simulation of the engine transient behavior during its starting phase required the addition of some elements to the engine configuration. The derived engine configuration is shown in Figure 7.5, while in Table 7.7, the elements that were added are presented in bold.

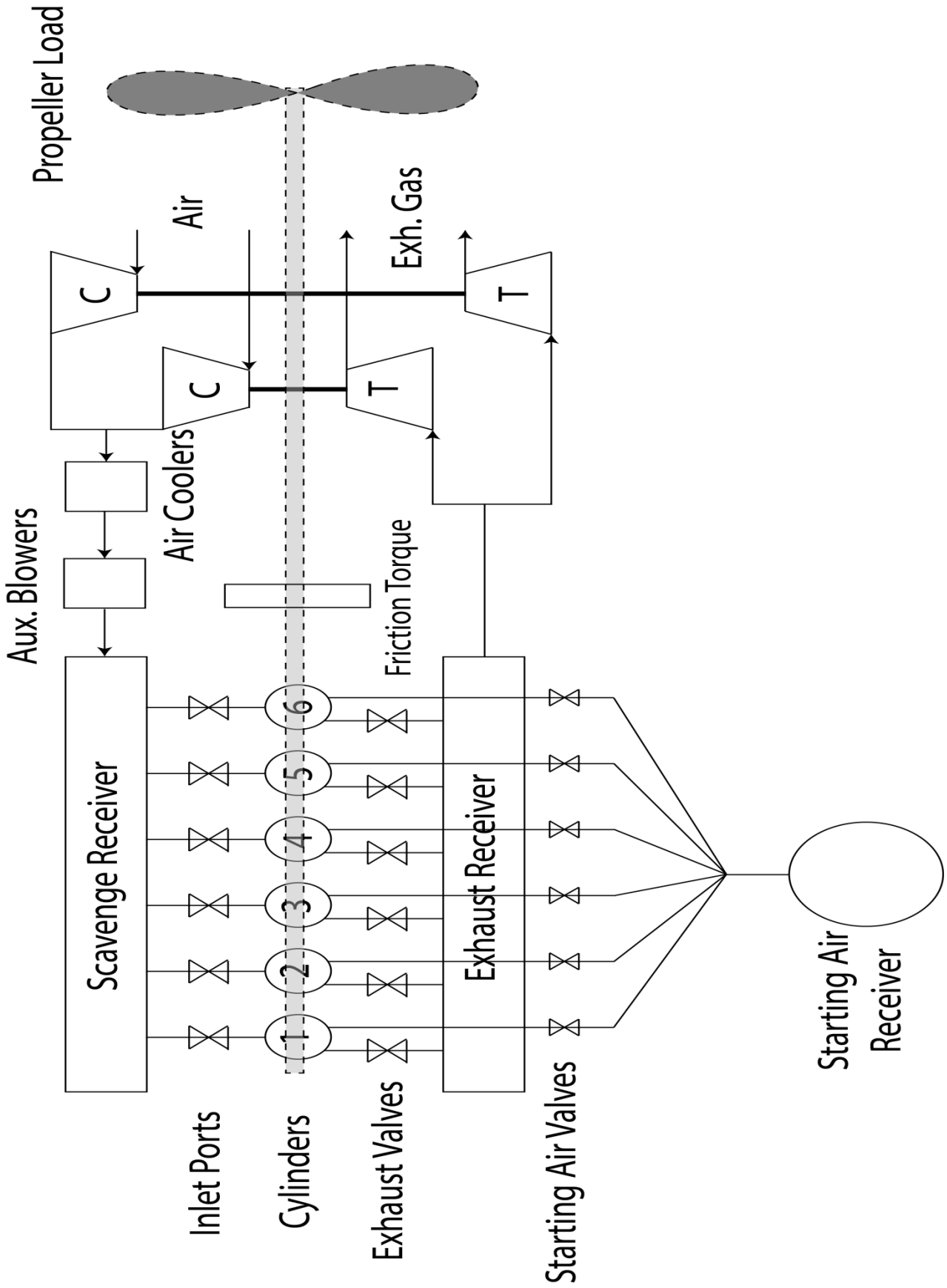

Figure 7.5: *Engine Configuration for the Simulation of its transient behavior during the Starting Phase*

Thermodynamic elements		Mechanical elements
Flow Receivers	**Flow Controllers**	
Scavenge receiver	Inlet ports	Crankshaft
Cylinders	Exhaust Valves	Turboshafts
Exhaust Receiver	Compressor	***Friction Torque Shaft load***
Inlet Fixed Fluid	Turbine	***Propeller Torque Shaft load***
Exhaust Fixed Fluid	***Starting Valves***	
Starting Air Receiver		

Table 7.7: *Thermodynamic and Mechanical Elements added to the initial Engine Configuration*

The Starting Air Receiver was modeled as a Flow Receiver element of constant volume. Its volume was set to be equal to the total volume suggested by the manufacturer in order to fulfill the requirement for 12 consecutive starts, concerning reversible engines. The equivalence ratio of the plenum's gas was set to zero, while the initial pressure of the starting air receiver was changed according to the objective of each simulation.

The Starting Valves were modeled as Flow Controller elements. Each cylinder was connected with the Starting Air Receiver using an independent Starting Valve (see Figure 7.5). The effective area of each Starting valve was modeled as a function of the crank angle, as shown in Figure 7.6. Lastly, Starting Valves were modeled as one-way valves in order to avoid the case of flow exiting the cylinder and entering the Starting Air Receiver.

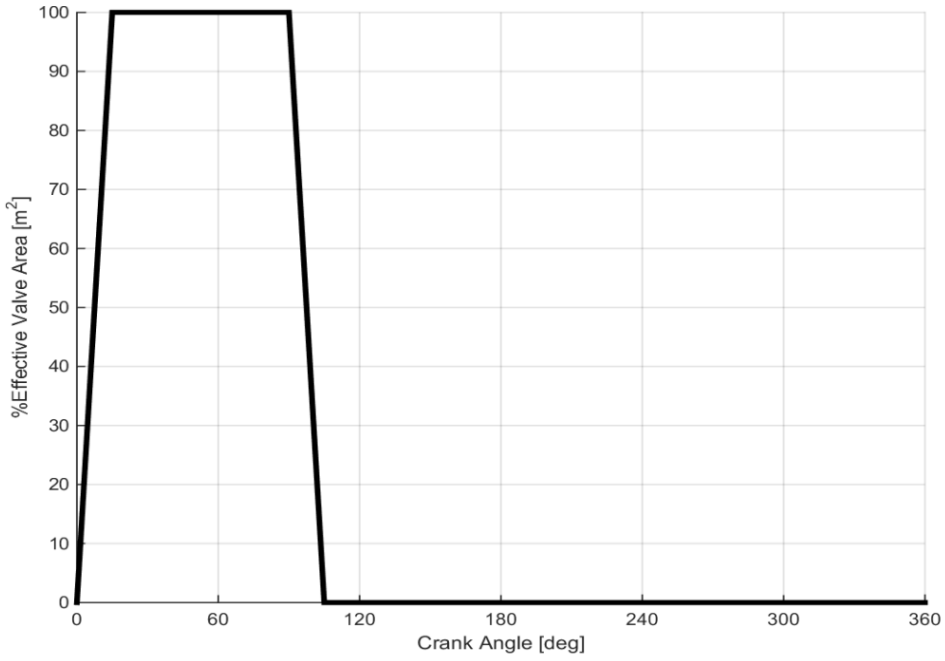

Figure 7.6: *Starting Valve Effective Area as a function of the Crank Angle*

The friction torque is modeled using a shaft load element connected to the crankshaft with zero polar moment of inertia. The friction torque is calculated at any instant as a function of the engine speed using equation (4.3.1). The static friction was derived from the maximum output torque of the turning gear's electric motor. The basic characteristics of the electric motor are presented in Table 7.8. The friction torque of the shafting system, as a function of the engine speed, is presented in Figure 7.7.

Output Speed	0.82 rpm (50Hz)
	0.98 rpm (60Hz)
Nominal Output Torque	42,969 Nm
Maximum Output Torque	58,525 Nm

Table 7.8: *Turning Gear Technical Data*

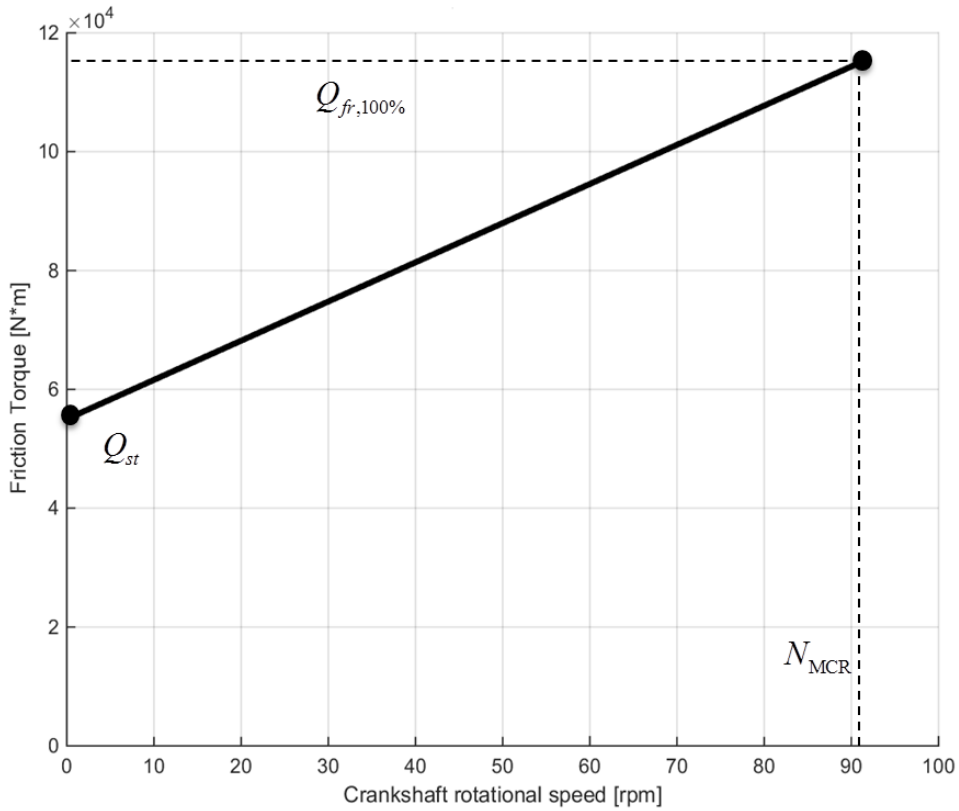

Figure 7.7: *Shafting System Frictional Torque Load*

Finally, it should be mentioned that the propeller load model, along with the ship surge model, were integrated to the MOTHER engine simulation code using an external subroutine, written in Fortran. The structure of the MOTHER allows the user to write an external subroutine in order to introduce new variables to the simulation. This subroutine is called by the main program at the beginning of each calculation step and was used for the calculation of the propeller performance characteristics and the ship's speed.

7.4 Simulation Results

First of all, a series of simulations were performed in order to validate the developed model. The initial pressure of the starting air receiver was changed to test the engine's ability to successfully start. The results are presented in Figure 7.8.

The engine starting simulation test proved to be successful if the initial pressure of the starting air receiver was set to 9 bar or above. The engine was unable to start if the initial pressure was set to be 7 bar or lower, instead. These results are in full compliance with the engine's shop trials concerning main engine starting test. According to the shop trials, the engine was unable to start when the pressure of the starting air receiver had dropped to 7.05 bar. During the simulations, the level of crankshaft revolutions for initial fuel injection was set to be 12% of the engine's MCR revolutions (see Figure 2.10).

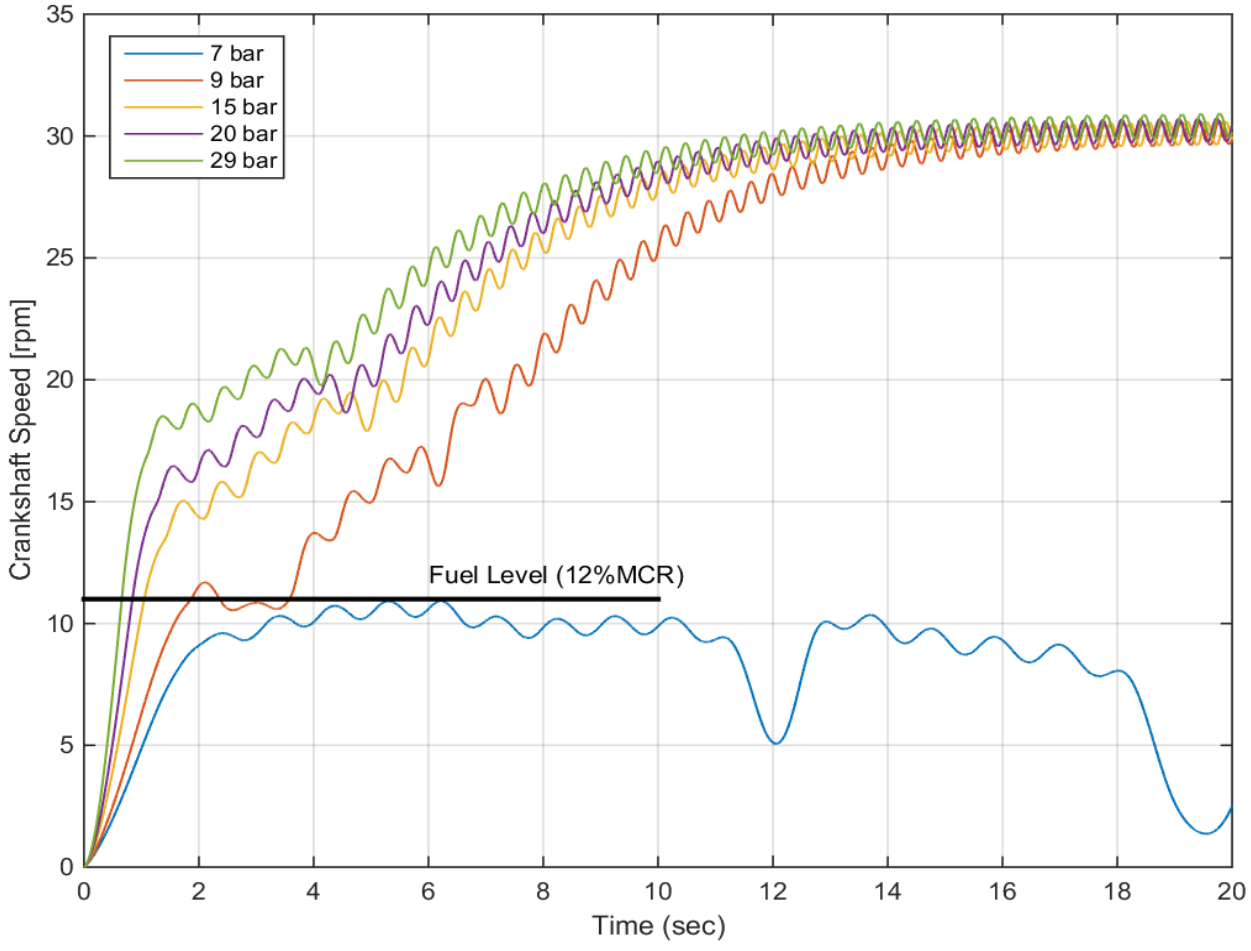

Figure 7.8: *Engine Starting Simulation Tests over a range of values for the initial Pressure of the Starting Air Receiver*

Then, a more detailed engine simulation was performed, during which the engine is started and then accelerated. The mass of fuel to be injected is gradually increased to the value corresponding to the engine's 25% steady state loading condition. The acceleration of the engine is shown in the following Figure 7.9, while the per cycle average operating points of the compressor, during the same simulation, are presented in Figure 7.10.

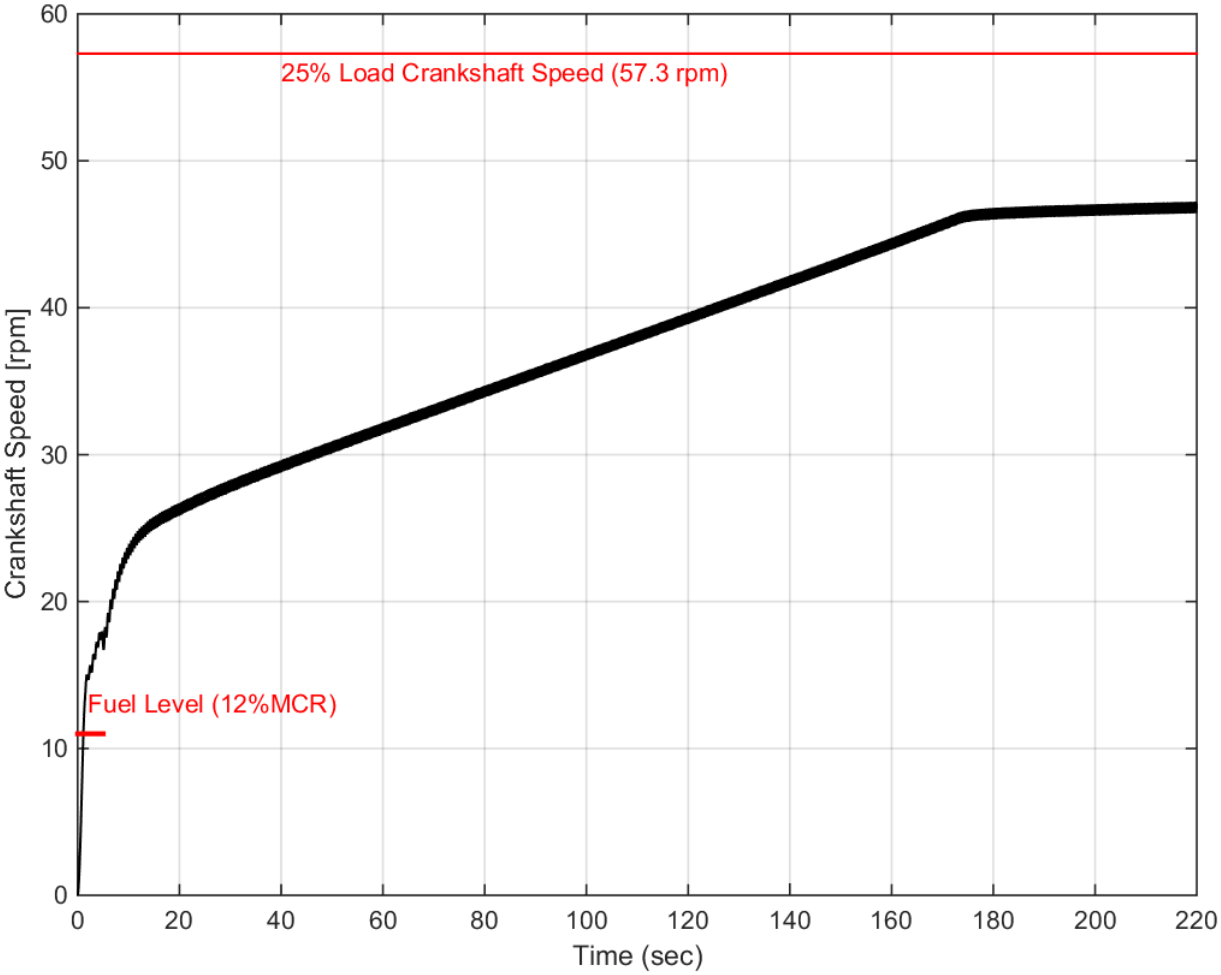

Figure 7.9: *Engine Starting and Acceleration Simulation*

In Figure 7.9, a large deviation of the engine speed compared to the one corresponding to the 25% steady state loading condition, can be observed. Despite the fact that the mass of fuel injected per cycle after about three minutes, is the same as the one derived from the steady state run for 25% load, the engine rotates at about 10 revolutions per minute less.

One cause is that the propeller torque demand is increased. The ship is accelerating slowly due to its large inertia and it's travelling at a very low speed. Thus, the advance speed is very low, resulting in a very low value of the advance angle β corresponding to a very high value of the propeller torque coefficient C_Q^*.

Another cause is the poor performance of the compressor, as shown in Figure 7.10. The initial pressure at the scavenge and the exhaust receiver is almost equal to the ambient pressure and it takes time to be increased. Part of the turbine power is also used to accelerate the turbocharger. Thus, the engine boost pressure will be lower than the one corresponding to steady state conditions.

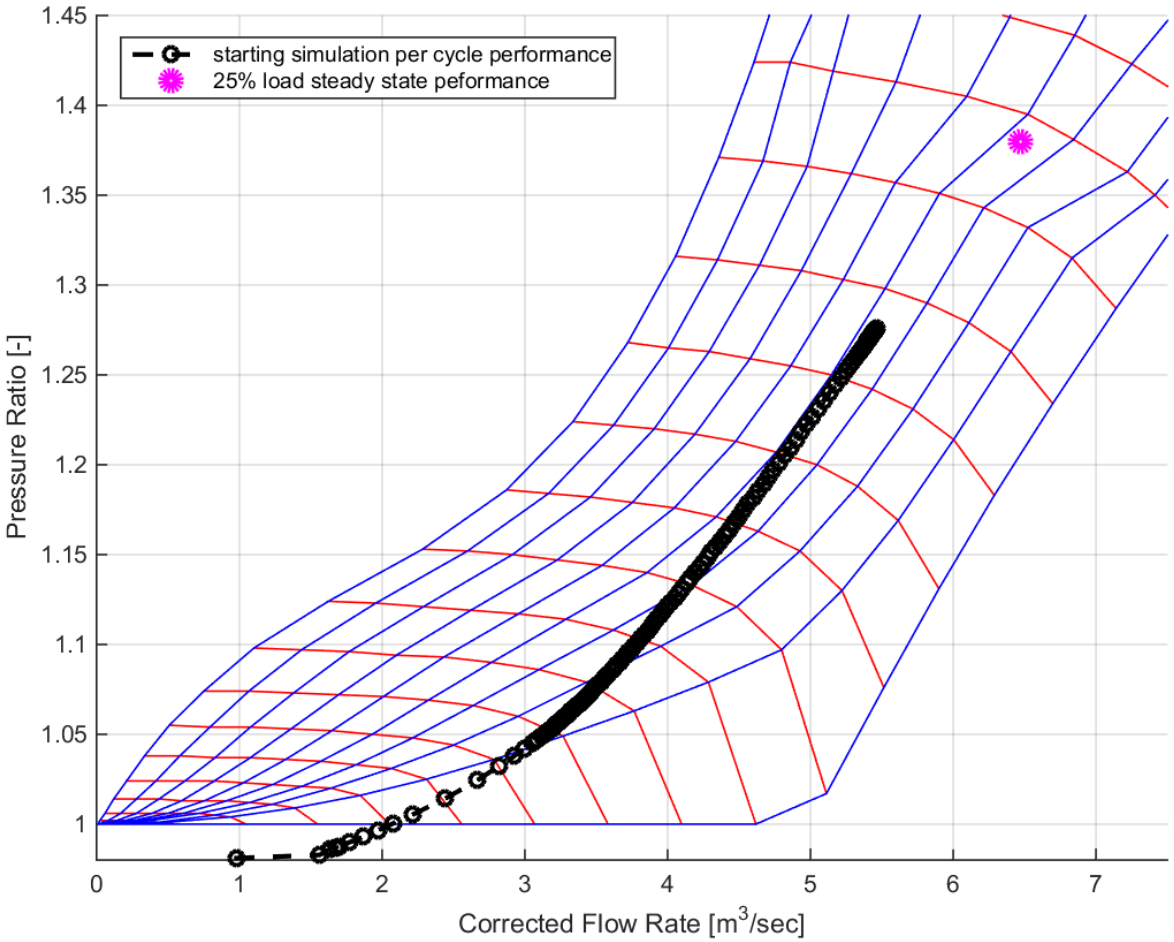

Figure 7.10: *Compressor Poor Performance during Engine Starting and Acceleration Simulation due to low Exhaust Receiver Pressure*

As the ship gradually accelerates, the advance speed and the advance angle also increase resulting in a lower propeller torque coefficient. Hence, the engine's operating point moves towards the one corresponding to the steady state conditions. This gradient transition, which takes about 40 minutes, is shown in the following Figure 7.11. This figure shows the engine - propeller – ship interaction for an accelerating ship with zero initial speed. The ship speed and the advance angle are increasing resulting in the decrease of the propeller torque coefficient and the engine – propeller torque equilibrium.

The compressor performance and its transition to the operating point corresponding to the steady state condition, during the same simulation, is also shown in Figure 7.12.

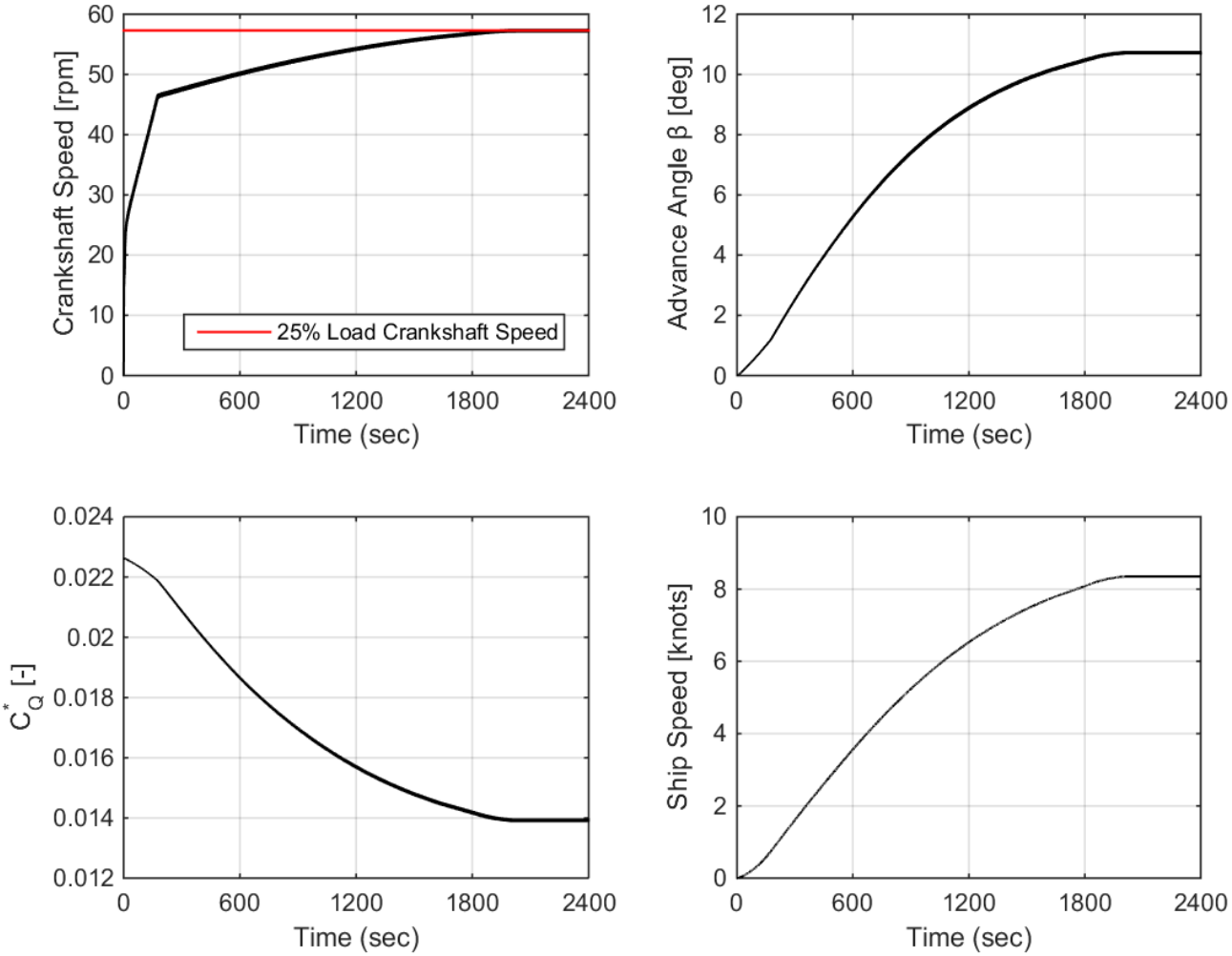

Figure 7.11: *Engine – Propeller – Ship Interaction during Starting and Acceleration Simulation*

Finally, a crash-stop manoeuvre simulation was performed and the engine - propeller dynamic interaction is presented using a Robinson diagram, as shown in Figure 7.13. The diagram consists of the propeller torque, relative to the propeller torque demand in design conditions, as a function of the shaft speed, relative to the shaft speed at MCR. At point “A” the stop command is send to the engine and the fuel supply is cut off. The engine speed drops very quickly to about 43 rpm (point “B”), while the speed of the ship remains practically unchanged due to the ship’s large inertia. The fast drop of the engine speed takes about 6 seconds, while the ship’s speed has dropped about one tenth of a knot.

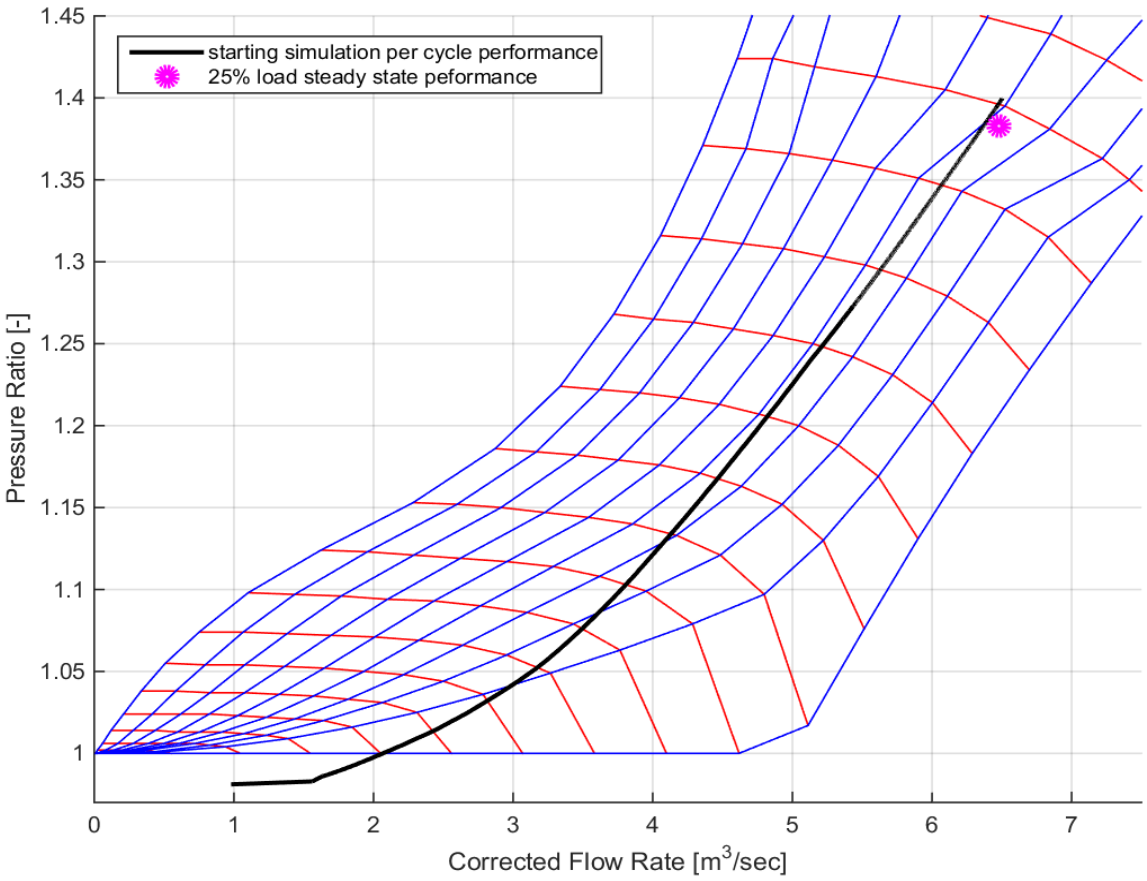

Figure 7.12: *Compressor Performance during Engine Starting and Acceleration Simulation*

From point "B" to point "C" the ship enters the coasting phase. During this phase the propeller operates as a Kaplan turbine, due to the fact that it rotates in the ship's wake flow. Hence, the propeller develops sufficient torque to rotate the engine in an off-design equilibrium. As the ship decelerates very slowly, the hull's wake flow velocity decelerates accordingly. Thus, reduced engine - propeller speed equilibrium is observed. Concerning ship's stopping distance, the coasting phase is the most critical during a crash – stop manoeuvre. The ship speed is still high, thus yielding the largest fraction of the stopping distance results. In this simulation the coasting phase lasted about 6 minutes and 40 seconds and the ship has covered a distance of about 2.5 kilometers.

The coasting phase of the crash-stop manoeuvre ends when the engine speed reaches the braking air level (point "C"), making it possible for compressed air to be admitted into the cylinders in order to brake the engine. Compressed air is admitted through the starting valves in astern direction timing, resulting in a very fast deceleration of the engine. The suggested range for braking air level revolutions is stated by the manufacturer (see Figure 2.10) to ensure safe engine operation. In the

current simulation the braking air level was set to 19 rpm, approximately 20.9% of the engine speed at MCR.

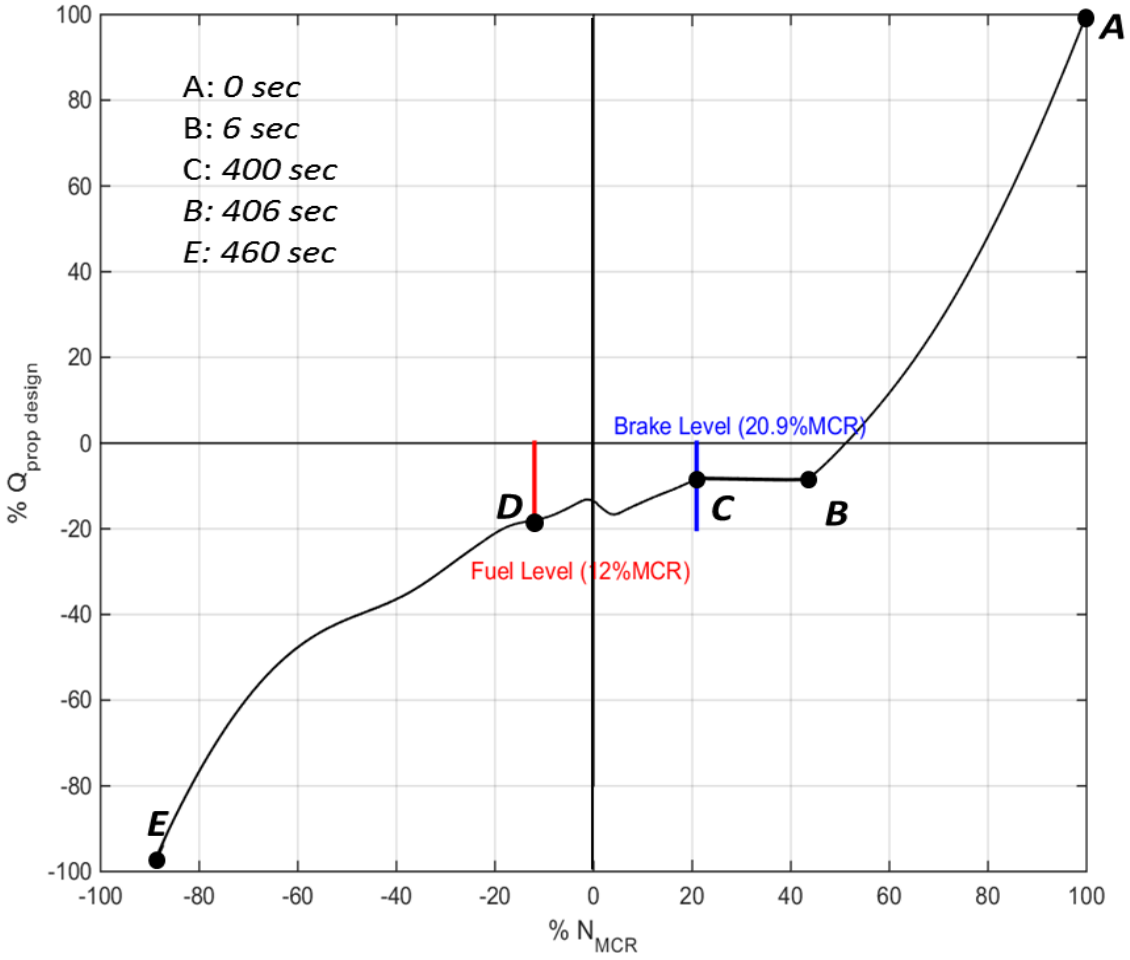

Figure 7.13: *Robinson Diagram for a Crash-Stop Manoeuvre*

After the engine reaches a complete stop, it is able to start in the astern direction. Compressed air is still being admitted into the cylinders to accelerate the engine in the reverse direction. When the engine reaches the fuel level revolutions in the opposite direction (point “D”), fuel is injected into the cylinders. The reversal of the engine has now been completed. The engine braking and reversing procedure takes about 6 seconds.

Finally, the engine can be accelerated to the maximum permissible astern revolutions for safe engine operation. In the current simulation the engine is accelerated to a maximum of 80 rpm, approximately 90% of the ahead MCR revolutions. The engine cannot reach the ahead MCR revolutions because of the propeller’s high torque demand. The propeller is still working in the wake flow of the ship hull which is moving in the ahead direction, while the propeller rotates in the astern direction. Nevertheless, the propeller now generates thrust in the astern direction causing the ship to a faster deceleration until it stops completely.

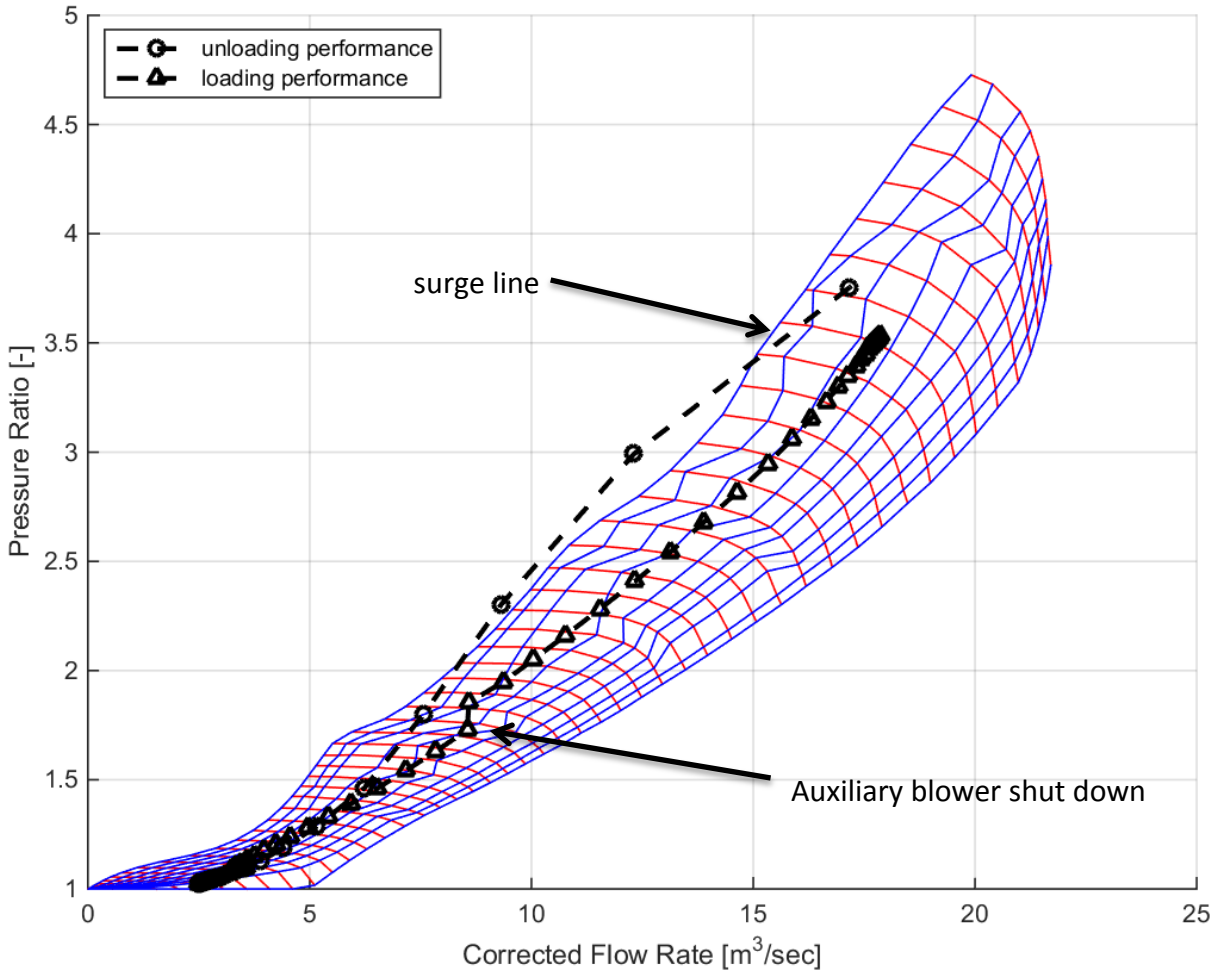

Figure 7.14: *Per Cycle Average Compressor Operating Points during Engine Crash-Stop Manoeuvre*

The operating points of the compressor, during the previously described crash-stop manoeuvre, are presented in Figure 7.14. During unloading, a large transition of the compressor operating points to the surge region is observed, while during engine's acceleration the compressor performance is smoother. Similar results for the compressor performance during engine's unloading were observed in [16].

This behavior can be explained in reference to Figure 7.15, which shows the per cycle average exhaust gas receiver temperature and the per cycle average scavenge receiver pressure for the first four cycles during engine's unloading. The exhaust gas receiver temperature drops rapidly when the fuel supply is cut off, while the pressure at the scavenge receiver drops at a lower rate. The rapid decrease of the engine speed results in a lower time averaged scavenge port available flow area. So, the flow rate decreases, but the pressure ratio is still high, during the first cycles.

The impact of the auxiliary blower operation on the compressor performance, is also shown in Figure 7.14. As long as the auxiliary blower is operating, the working pressure ratio of the compressor is lower. That enables the compressor's operating

points to move to points corresponding to higher flow rates for the same compressor speed. This observation is a direct result of the auxiliary blower operation being modeled as a static pressure increase of the compressed air exiting the compressor.

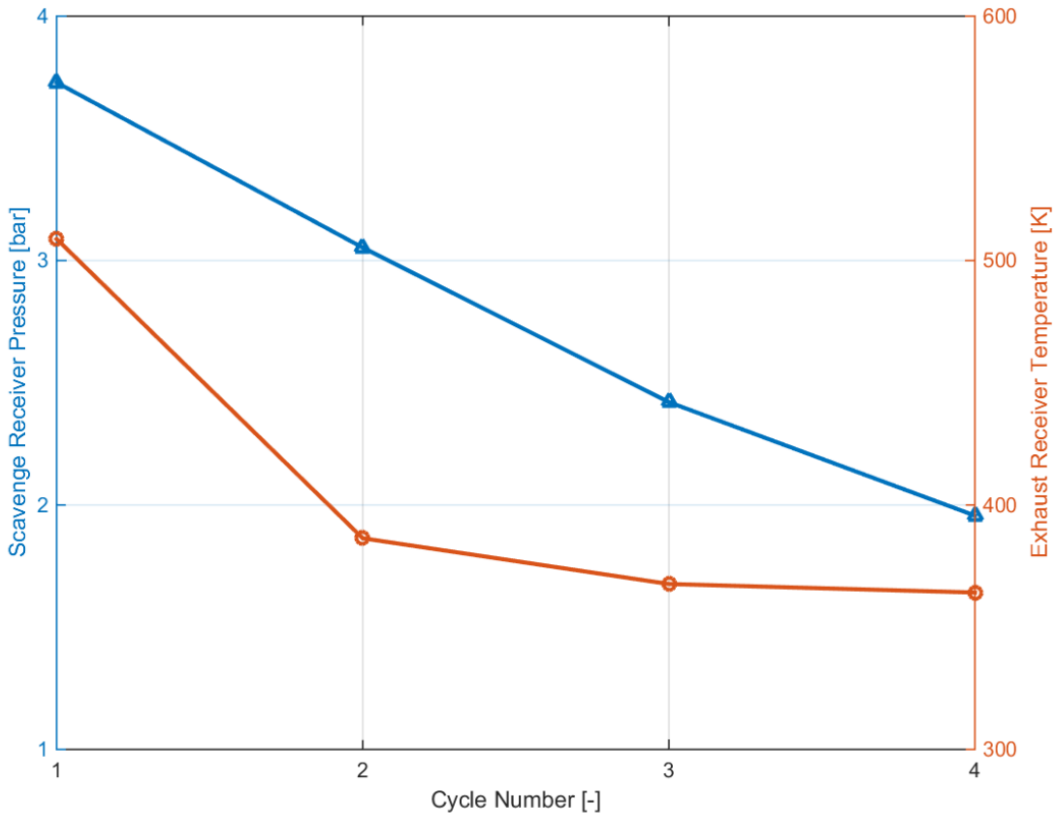

Figure 7.15: *Per Cycle Average Temperature and Pressure Drop, in Exhaust and Scavenge Receiver, respectively*

8 Conclusions

8.1 Discussion

The present thesis focused on the modeling of the starting system of a large two-stroke diesel engine with direct admission of compressed air into the cylinders through a separate starting valve fitted on each cylinder.

In this respect, a model capable of predicting the transient behavior of the engine during its starting phase was developed. The turbocharger performance prediction, during this phase, was based on the extrapolation of the compressor and turbine maps for low load operation. The impact of the poor turbocharger performance on the transient behavior of the engine was also examined.

The main findings of this work are summarized as follows:

The developed model is able to predict the dynamic behavior of a turbocharged propulsion engine during its initial starting phase.

The engine performance during this phase is limited by the poor performance of the turbocharger. The pressure in the exhaust receiver is not sufficient to power the turbine, which cannot support the compressor's torque demand.

Furthermore, the engine – propeller – ship interaction was found to be very important during the starting phase of the engine. Due to the ship's large inertia, its speed increases at a very low rate, resulting in high values of the propeller torque coefficient. As a result, the propeller's torque demand is increased compared to the one corresponding to steady state conditions.

The crash – stop manoeuvre simulation showed that during fast deceleration of the engine, the compressor performance might become unstable. The operating points of the compressor move to the surge region because of the faster pressure drop at the exhaust receiver than the one at the scavenge receiver and the inertia of the turbocharger.

Lastly, the integration of the developed models into the MOTHER engine simulation and performance prediction code enables the incorporation of models for other engine sub-systems. In this respect, the performance of such systems can be evaluated during the starting phase of the engine.

8.2 Recommendations for Future Research

The prediction of the transient behavior of the engine during its starting phase is quite complicated. It requires the accurate prediction of the interaction between all the components involved. Briefly, the future research should be concentrated on the following:

- The adaptation of the model used to predict the compressor – auxiliary blower interaction during the starting phase of the engine.
- The introduction of a pipe element in the MOTHER engine simulation code to enable the calculation of the pressure drop in piping systems. This element will be used to connect flow receivers to flow controllers.
- The incorporation of a governor to the current engine configuration in order to enable the more accurate simulation of the engine acceleration.
- The modeling and incorporation of other engine peripheral systems into the current engine configuration in order to evaluate their performance during the starting phase of the engine.

References

[1] MAN B&W, "*MAN B&W S70MC-C7 Project Guide – Camshaft Controlled Two - Stroke Engines*", 4th Edition, January 2009

[2] MAN B&W, "*Uni - concept Auxiliary Systems for Two – Stroke Main Engines and Four – Stroke Auxiliary Engines*"

[3] American Bureau of Shipping (ABS), "Part 4 – Vessel Systems and Machinery", Rules for Building and Classing Steel Vessels, 2011

[4] Theotokatos Gerasimos, "*Analysis of Turbocharger Operation including Compressor Surging during Transient Loading of Marine Diesel Engines*", PhD thesis, National Technical University of Athens, May 2001

[5] Kyrtatos N. P., "*Motor THERmodynamics – USER MANUAL*", Version 2.1, January 2013

[6] Armstrong – Hélouvry Brian, "*Control of Machines with Friction*", Springer, 1991

[7] Gua Cong, Theotokatos Gerasimos, Zhou Peilin, Hui Chen, "*Computational investigation of a large containership propulsion engine operation at slow steaming conditions*", Applied Energy, 2014, Vol. 130, pp. 370 - 383

[8] Moraal Paul, Kolmanovsky Ilya, "*Turbocharger Modeling for Automotive Control Applications*", Society of Automotive Engineers, 1999

[9] Erikson L., "*Modeling and Control of Turbocharged SI and DI Engines*", Oil & Gas Science and Technology, 2007, Vol. 62, pp. 523 - 538

[10] Jensen J. P., Kristensen A. F., Sorenson S.C., Houbak N., "*Mean Value Modeling of a Small Turbocharged Diesel Engine*", SAE Technical Papers, 1991

[11] MAN B&W, "*Basic Principles of Ship Propulsion*", September 2013

[12] Andreas Torp Karlsen, "*On modeling of a Ship Propulsion System for Control Purposes*", Master thesis, Norwegian University of Science and Technology, June 2012

[13] Carlton John, "*Marine Propellers and Propulsion*", Second Edition, Elsevier, 2007

[14] MacPherson Donald, Puelo Vincent, Packard Matthew, "*Estimation of Entrained Water Added Mass Properties for Vibration Analysis*", SNAME New England Section, 2007

[15] Robert F. Roddy, David E. Hess, Will Faller, "*Neural Network Predictions of the 4-Quadrant Wageningen Propeller Series*", Hydromechanics Department, David Taylor Model Basin, 2006

[16] Kyrtatos N., Koumbarelis I., "*Performance prediction of next generation slow speed diesel engines*", trans IMarE, 1993, Vol. 106